Compact Reduced-Order Modeling of Weakly Nonlinear Analog and RF Circuits

Peng Li, *Member, IEEE,* and Lawrence T. Pileggi, *Fellow, IEEE*

***Abstract*—A compact nonlinear model order-reduction method (NORM) is presented that is applicable for time-invariant and periodically time-varying weakly nonlinear systems. NORM is suitable for model order reduction of a class of weakly nonlinear systems that can be well characterized by low-order Volterra functional series. The automatically extracted macromodels capture not only the first-order (linear) system properties, but also the important second-order effects of interest that cannot be neglected for a broad range of applications. Unlike the existing projection-based reduction methods for weakly nonlinear systems, NORM begins with the general matrix-form Volterra nonlinear transfer functions to derive a set of minimum Krylov subspaces for order reduction. Moment matching of the nonlinear transfer functions by projection of the original system onto this set of minimum Krylov subspaces leads to a significant reduction of model size. As we will demonstrate as part of comparison with existing methods, the efficacy of model reduction for weakly nonlinear systems is determined by the achievable model compactness. Our results further indicate that a multipoint version of NORM can substantially improve the model compactness for nonlinear system reduction. Furthermore, we show that the structure of the nonlinear system can be exploited to simplify the reduced model in practice, which is particularly effective for circuits with sharp frequency selectivity. We demonstrate the practical utility of NORM and its extension for macromodeling weakly nonlinear RF communication circuits with periodically time-varying behavior.**

***Index Terms*—Analog circuits, modeling, model order reduction, nonlinearity, RF circuits.**

I. Introduction

OVER the past decade a large body of work on model order reduction of IC interconnect has emerged from the design automation community [1]–[7]. The purpose of model reduction is to generate models that are orders of magnitude smaller than the original system, while accurately approximating the input–output relationships of the original system. Compared to the success of model order reduction for linear time invariant (LTI) resistance–inducatance–capacitance networks, the problem of reducing nonlinear systems has been less understood and explored [8]–[10].

Manuscript received August 11, 2003; revised January 21, 2004. This work was supported in part by the Semiconductor Research Corporation under Contract 2000-TJ-779. This paper was recommended by Associate Editor C.-J. R. Shi.

P. Li was with the Department of Electrical and Computer Engineering, Carnegie Mellon University, Pittsburgh, PA 15213 USA. He is now with the Department of Electrical Engineering, Texas A&M University, College Station, TX 77843 USA (e-mail: pli@neo.tamu.edu).

L. T. Pileggi is with the Department of Electrical and Computer Engineering, Carnegie Mellon University, Pittsburgh, PA 15213 USA (e-mail: pileggi@ece.cmu.edu).

Digital Object Identifier 10.1109/TCAD.2004.837722

There are numerous applications, however, where abstracting transistor-level circuit details that include important weakly nonlinear effects into a compact macromodel is important. For instance, in RF communication IC design there is a growing interest in extracting efficient circuit-level models which are capable of capturing system nonlinear distortion. While circuit blocks in these applications often exhibit weak nonlinearities, the design specification for linearity is often extremely important and very stringent. As depicted in Fig. 1, building compact blackbox type macromodels that accurately capture nonlinear input–output correspondence not only facilitates efficient repetitive simulations of the circuit component being modeled, but also enables the entire-system verification that would otherwise be impossible.

In terms of nonlinear model generation or reduction, symbolic modeling of weakly nonlinear circuits has been used to build system-level models [22], [23], [30], [31]. The underlying mathematical description employed is Volterra series (e.g., [12]–[14]), and the resulting model is in a block-diagram form suitable for signal-flow type simulation using tools such as Matlab Simulink [19]. Neural network and time series-based models have also been proposed for nonlinear behavioral modeling. A review of the related work can be found in [28].

In a different direction, transformation-based model order reduction techniques have been stimulated by the progress made for model order reduction of large linear IC interconnects in the past decade (e.g., [1]–[7]). A piecewise-linear approximation based nonlinear systems reduction was proposed in [11], where a set of linearizations about the state trajectory due to a training input was used to model a nonlinear system and each linearization is reduced using Krylov projection. While having the potential capability of handling large nonlinearities, the limitation of this approach is its training-input dependency. This piecewise-linear approximation was recently extended to a piecewise-polynomial approach to better model nonlinear distortion [27].

For a broad class of weakly nonlinear systems in analog signal processing and RF communication ICs, the low distortion level, as well as the required modeling accuracy, seemingly makes Volterra series a more suitable choice for system description. The application of Volterra series makes it possible to solve the circuit response of a weakly nonlinear system from low orders to high orders via a recursive procedure, commonly referred to as *nonlinear current method*. More importantly, frequency-domain characterizations based on Volterra kernels or nonlinear transfer functions fully describe the input-independent system nonlinear properties in a manner analogous to the use of linear transfer functions for linear system properties. The

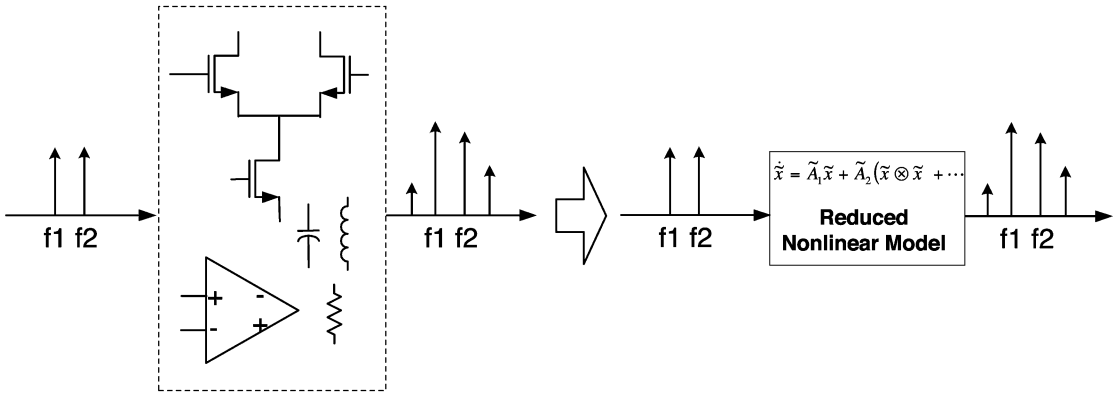

Fig. 1. Macromodeling of nonlinear circuits.

projection-based nonlinear model order-reduction frameworks for weakly nonlinear systems were first proposed in [8]–[10] by extending the popular implicit moment-matching projection techniques used for interconnects, such as PVL [3], the Arnoldi method [4], and PRIMA [6]. The work of [8] and [10] uses the Taylor series expansion of nonlinear state equations to represent a weakly nonlinear system. Then, the nonlinear system model inherited in the recursive nonlinear current method is employed to view a weakly nonlinear system as a set of interconnected linear networks. Some details of this direction is presented in [26].

The benefit of this perspective is that it immediately allows the use of existing linear system-reduction techniques to serve as blackbox tools to reduce each individual linear network for achieving the goal of overall nonlinear system reduction. However, converting a nonlinear reduction problem to several linear reduction problems leaves several important issues unaddressed. First, it becomes not clear that how the quality of each linear reduction problem impacts the accuracy of the overall nonlinear model. Second, the approach does not provide strategies for optimizing the reduced nonlinear model.

Another approach [9], which provides an interesting theoretical foundation, uses the bilinear form of a nonlinear system and matches the moments of nonlinear transfer functions analogously to Padé approximations of LTI systems. The use of bilinear form allows the nonlinear transfer function moments to be expressed in a very structured fashion such that a projection-based moment-matching reduction scheme can be elegantly derived. The critical issue associated with this approach is that by converting a standard state-equation form to its bilinear counterpart, a large number of additional state-variables are introduced. For instance, the bilinear form of a system including up to the third-order nonlinear coefficient matrices has $O(N^3)$ state variables, where N is the number of state variables in the original state-equation form.

It is very important to note that under the projection framework, the reduced model compactness is critical for effective nonlinear model reduction. This is because as the order of moment-matching increases, the size of the reduced order model increases even more rapidly. At the same time, as the size of the reduced model grows, it becomes increasingly costly to explicitly form the resulting high-order system matrices of the reduced order model, thereby eliminating any possible benefit of model reduction.

Given that the primary limitation is the size of the reduced order models, we have proposed a different path for producing more compact reduced order models for nonlinear systems in [18] and [19]. The proposed projection-based nonlinear model order-reduction techniques start from the same Volterra formulation for weakly nonlinear systems. However, our approach possesses the following key differences from the prior work. Unlike the method in [8] and [10], where moment matching of nonlinear transfer functions are not explicitly considered, as well as the approach in [9], where large bilinear forms are used, we begin with the most general matrix-form nonlinear transfer functions needed for model order reduction. To disclose the problem structure of nonlinear model order reduction, moments of nonlinear transfer functions and associated Krylov subspaces are further derived in the matrix form. This development leads to a deeper understanding on the interaction between Krylov subspace projection and the moment matching under nonlinear context. As has been experienced in model order reduction of linear systems, we will show in this paper that efficient (implicit) moment matching of nonlinear transfer functions can lead to compact nonlinear reduced order models. Our analysis allows us to establish an optimal link between moment matching and Krylov subspace projection. The efficiency of the proposed nonlinear model order-reduction method (NORM) scheme is based on an optimal construction of the projection matrix. Under the projection framework, NORM produces the optimized reduced order models in the sense that any given number of nonlinear transfer function moments can be matched by projecting the original nonlinear system onto a set of minimum Krylov subspaces. As a result, a significant improvement on model compactness is achieved, which is essential to nonlinear model order reduction. In this paper, we extend our work in [18] and [19] to a complete reduced-order modeling methodology for weakly nonlinear analog and RF circuits. In particular, the expressions of nonlinear transfer function moments, which are essential to the proposed algorithms, are fully derived. We also prove the moment matching property of the proposed NORM algorithm. Furthermore, we extend our nonlinear system formulation to periodically time-varying systems and demonstrate that time-varying circuits can be modeled under the same framework.

The proposed NORM algorithm has several important features for controlling the growth of reduced order models. First, the modeling accuracy for the nonlinear effect at each order can be selected individually for application-specific needs, while the overall reduced nonlinear model is optimally constructed based on the interactions of moment matching for nonlinear transfer functions of different orders. This is important, as it avoids the introduction of useless projection vectors for moment matching, which can potentially be the case in the method of [8] and [10]. Second, to target the nonlinear system behavior within the circuit-specific frequency band of interest, the procedure for moment-matching with complex expansion points is accommodated. This is particularly useful for certain narrow-band RF systems for which it is beneficial to expand the nonlinear transfer functions along the imaginary axis about the center frequency. Different from the reduction of the LTI system, it is shown that moment matching of nonlinear transfer functions at a single frequency expansion point inherits multiple matrix factorizations. Therefore, special care must be taken in order to perform the task correctly. Lastly, it is shown that multipoint expansions for projection-based nonlinear model order reduction has a very unique advantage against single-point approaches in terms of model compactness. By trading off computational cost with model compactness, we demonstrate that a multipoint version of the NORM algorithm can further reduces the total dimension of the Krylov subspaces used in the projection, thereby producing a more compact model.

For systems with sharp frequency selectivity, such as high-Q circuits, a full projection-based approach can still be limited by the need of forming the reduced high-order system matrices. This is due to the fact that a large number of projection vectors may be required to model the nonlinear system frequency domain characteristics accurately in the band of interest, leading to large and dense reduced high-order matrices. To overcome this difficulty, in this paper, we further explore a novel hybrid approach where the benefits of nonlinear Padé approximations and pruning by exploitation of the system's internal structure are combined. In this hybrid approach, the low-order system nonlinear responses are captured efficiently using the aforementioned projection-based NORM algorithm, while high-order responses (third order) are approximated via direct matrix pruning, in conjunction with the projection-based reduction of a linear adjoint network [19]. The pruning technique is similar to what was used in symbolic modeling [22], [23], [30], [31], with the difference being that the pruning is applied directly to the high-order system matrices in our approach, and the model order reduction is embedded with the pruning to accelerate this relatively slow procedure.

This paper is organized as follows. In Section II, we present a brief introduction to the time-invariant Volterra series used for time-invariant systems. The prior nonlinear reduction approach of [8] and [10] is reviewed for comparison purposes in Section III. In Section IV, we present the general matrix-form nonlinear transfer functions for time-invariant systems, and derive the expressions for the corresponding transfer function moments used in NORM. The NORM algorithm is discussed in detail in Section V. In Section VI, the hybrid approach is presented. We demonstrate the accuracy of reduced-order models generated via NORM and the proposed hybrid approach, and show the orders of magnitude runtime speedup that is possible in simulation for several circuit examples in Sections V-D and VI-C. Finally, conclusions are drawn in Section VII. The extension to the model order reduction of periodically time-varying weakly nonlinear systems is presented in the Appendix.

II. Background on Volterra Series

For simplicity, consider a single-input multioutput system described by the following modified nodal analysis (MNA) formulation

$$f\big(x(t)\big) + \frac{d}{dt}\Big(q\big(x(t)\big)\Big) = bu(t), \qquad y(t) = D^T x(t) \quad (1)$$

where $x \in R^n$ is the vector of node voltages and branch currents; u is the input to the system, $f(\cdot)$ and $q(\cdot)$ are nonlinear functions relating currents of nonlinear resistors and nonlinear charges/fluxes with x; y is the vector of the output; b and D are the input and output matrices, respectively. Assume that the weakly nonlinear system is perturbed about a dc bias condition x_0 by a small-signal input. Using a Taylor series to expand $f(\cdot)$ and $q(\cdot)$ at the bias point x_0, and considering only small-signal quantities, we obtain

$$\begin{aligned}&\frac{d}{dt}(C_1 x + C_2(x \otimes x) + C_3(x \otimes x \otimes x) + \cdots)\\ &\quad + G_1 x + G_2(x \otimes x) + G_3(x \otimes x \otimes x) + \cdots = bu(t) \quad (2)\end{aligned}$$

where $\otimes$ is the Kronecker (tensor) product operator, $x(t)$ and $u(t)$ are the small-signal response and the input of the system.

$$G_i = \frac{1}{i!}\left.\frac{\partial^i f}{\partial x^i}\right|_{x=x_0} \in R^{n\times n^i}, \qquad C_i = \frac{1}{i!}\left.\frac{\partial^i q}{\partial x^i}\right|_{x=x_0} \in R^{n\times n^i}$$

are the ith-order conductance and capacitance matrices, respectively.

A nonlinear system can be analyzed using Volterra functional series under weakly nonlinear conditions. In Volterra series, the response $x(t)$ can be expressed as a sum of responses at different orders

$$x(t) = \sum_{n=1}^{\infty} x_n(t) \quad (3)$$

where x_n is the nth-order response. In an intuitive sense, the order of a response component specifies the cumulative number of multiplications of the input signal for resulting the corresponding response. In practice, a converging Volterra series of (3) is truncated to a finite number of terms, and each order of response is solved recursively. The first order or linear response of the weakly nonlinear system in (2) is obtained simply by retaining only first-order terms in (2)

$$\frac{d}{dt}\big(C_1 x_1(t)\big) + G_1 x_1(t) = bu(t). \quad (4)$$

Notice that (4) represents a linear time-invariant (LTI) system. Higher order responses are computed by solving the linearized

system with different inputs. The second- and the third-order responses are given by the following two equations, respectively:

$$\frac{d}{dt}(C_1x_2)+G_1x_2=\frac{d}{dt}(C_2(x_1\otimes x_1))-G_2(x_1\otimes x_1) \quad (5)$$

$$\frac{d}{dt}(C_1x_3)+G_1x_3=-G_3(x_1\otimes x_1\otimes x_1)-2G_2(\overline{x_1\otimes x_2}) - \frac{d}{dt}\big(C_3(x_1\otimes x_1\otimes x_1)+2C_2(\overline{x_1\otimes x_2})\big) \quad (6)$$

where $(\overline{x_1\otimes x_2})\equiv(1/2)((x_1\otimes x_2)+(x_2\otimes x_1))$. We shall refer to the systems specified by (4) –(6) as the linearized (first-), second- and third-order systems for (2), respectively.

More formally, the nth-order response can be related to *Volterra kernel of order* $n, h_n(\tau_1,\ldots,\tau_n)$, which is an extension to the impulse response function of an LTI system

$$x_n(t)=\int_{-\infty}^{\infty}\cdots\int_{-\infty}^{\infty}h_n(\tau_1,\ldots,\tau_n) \times u(t-\tau_1)\ldots u(t-\tau_n)\,d\tau_1\ldots d\tau_n. \quad (7)$$

Alternatively, a weakly nonlinear system can be analyzed in the frequency domain, where $h_n(\tau_1,\ldots,\tau_n)$ is transformed into the frequency domain via Laplace transform

$$H_n(s_1,\ldots,s_n)=\int_{-\infty}^{\infty}\cdots\int_{-\infty}^{\infty}h_n(\tau_1,\ldots,\tau_n) \times e^{-(s_1\tau_1+\cdots+s_n\tau_n)}\,d\tau_1,\ldots,d\tau_n. \quad (8)$$

In (8), $H_n(s_1,\ldots,s_n)$ is referred to as the *nonlinear transfer function of order* n. The nth-order response, x_n, can also be related to the input using $H_n(s_1,\ldots,s_n)$.

It can be seen that Volterra kernels and nonlinear transfer functions specify the weakly nonlinear system response due to an arbitrary input. Thus, they are input-independent properties of the system, and fully describes the weakly nonlinear system behaviors. As such, if the original nonlinear transfer functions are well approximated in a reduced order model using a method such as moment matching, it would be well expected that original nonlinear system properties are accurately modeled by the reduced model.

III. Prior Reduction Techniques

A projection-based nonlinear model order reduction approach was proposed in [8] and [10], where reduction techniques for LTI systems were properly extended to take the weakly nonlinear aspects of a system into consideration. For simplicity of description, consider the expanded state-space model of the nonlinear system in (1)

$$\frac{dx}{dt}=A_1x+A_2(x\otimes x)+A_3(x\otimes x\otimes x)+\cdots+bu. \quad (9)$$

Similar to (4)–(6), the first-order through the third-order nonlinear responses of the system are given by

$$\dot{x}_1=A_1x_1+bu \quad (10)$$

$$\dot{x}_2=A_1x_2+A_2(x_1\otimes x_1) \quad (11)$$

$$\dot{x}_3=A_1x_3+2A_2(\overline{x_1\otimes x_2})+A_3(x_1\otimes x_1\otimes x_1). \quad (12)$$

The key observation is that (10)–(12) represent three LTI systems with inputs formed by $u, x_1\otimes x_1$, and $[(\overline{x_1\otimes x_2})^T,(x_1\otimes x_1\otimes x_1)^T]^T$, respectively. Each of these LTI systems can be, in turn, reduced to a smaller system using any existing projection method such as that of [3]–[6]. If the system in (10), with n states, is reduced to a system with q_1 states through a Krylov subspace projection $x_1=V_{q1}\cdot\bar{x}_1$, then the inputs to (11) can be approximated by

$$x_1\otimes x_1\approx(V_{q1}\cdot\bar{x}_1)\otimes(V_{q1}\cdot\bar{x}_1)=(V_{q1}\otimes V_{q1})\cdot(\bar{x}_1\otimes\bar{x}_1). \quad (13)$$

This suggests that (11) now can be viewed as having q_1^2 inputs instead of n^2 inputs, and can be reduced by a Krylov projection $x_2=V_{q2}\cdot\bar{x}_2$ to a smaller system with q_2 states. Now, the number of inputs to (12) is reduced from n^2+n^3 to $q_1^3+q_1q_2$. Finally, (12) can be reduced to a smaller LTI system with q_3 states via projection $x_3=V_{q3}\cdot\bar{x}_3$. The final reduced nonlinear model can either be expressed in the form of a collection of reduced linear systems, or be described by a smaller set of nonlinear equations using variable embedding $x=V\cdot\bar{x}$, where V is an orthonormal basis of $[V_{q1},V_{q2},V_{q3}]$, and $\bar{x}\in R^{(q_1+q_2+q_3)\times1}$ are the states of the final reduced nonlinear model. For the latter case, for instance, the third-order matrix is reduced to a matrix of a smaller dimension as $\bar{A}_3=VA_3(V\otimes V\otimes V)$. It is important to note that the reduced third order matrix is usually dense and has $O(q^4)$ entries, where q is the number of states of the reduced model. Therefore, achieving model compactness is crucial for effective model reduction.

The obvious advantage of the above approach is that existing LTI techniques can be applied directly as a blackbox tool, but there are three major problems associated with this direct extension to LTI-based techniques. First, this approach reduces a weakly nonlinear system by approximating the underlying linear subsystems. The assumption is that the overall nonlinear behavior of the original system will be closely replicated in the reduced system if the corresponding linear circuits are well approximated. Nevertheless, it is difficult to assess the accuracy of the nonlinear system reduction, since it remains unclear that how the qualities of reduced linear subsystems interact with the quality of the reduced nonlinear model. Furthermore, there is a lack of guidance on how to optimize nonlinear model quality by choosing appropriate orders for the reduced linear models. Second, it can be seen that this method models a nonlinear system, potentially with small number of inputs, as several linear systems with many more inputs. Intuitively, this increase of degrees of freedom leads to unnecessarily large reduced models. Finally, the published work in [8] and [10] does not explicitly explore the flexible selection of expansion points for approximating nonlinear transfer functions. For instance, to capture accurately the third-order intermodulation around the

center frequency f_0 of a narrow-band amplifier, it might be desirable to expand the third transfer function $H(s_1, s_2, s_3)$ at expansion point $(j2\pi f_0, j2\pi f_0, -j2\pi f_0)$. To correctly perform the moment matching under this case, an understanding in the interdependency between nonlinear transfer functions of different orders is required. We will address these issues in detail as we present the proposed nonlinear model reduction algorithm NORM in the following sections.

IV. Matrix-Form Nonlinear Transfer Functions and Moments

To derive an efficient model order-reduction methodology for weakly nonlinear systems, an understanding of Volterra nonlinear transfer functions is needed. In this section, we will first derive the general matrix-form nonlinear transfer functions suitable for model order reduction. In what follows, nonlinear transfer-function moments will also be cast in a matrix form. Without loss of generality, we consider the MNA formulation for a single-input multioutput (SIMO)-based weakly nonlinear system in (1) and its expanded form in (2). The nonlinear transfer functions presented here are the corresponding matrix-form expressions of the analytical nonlinear current method used for computing Volterra kernels in [13] and [14]. Before proceeding, we first introduce the notations used throughout this paper. For matrices in (2) we define

$$\begin{aligned} A &= -G_1^{-1}C_1 \\ r_1 &= G_1^{-1}b \\ r_2 &\equiv r_1 \otimes r_1 \\ r_3 &\equiv r_1 \otimes r_1 \otimes r_1 \end{aligned} \tag{14}$$

and for an arbitrary matrix F, we define

$$\begin{aligned} F^{l\otimes m\otimes\cdots\otimes n} &\equiv F^l \otimes F^m \otimes \cdots \otimes F^n \\ \overline{F^{l\otimes m}} &\equiv \frac{1}{2}(F^{l\otimes m} + F^{m\otimes l}) \\ \overline{F^{l\otimes m\otimes n}} &\equiv \frac{1}{6}(F^{l\otimes m\otimes n} + F^{l\otimes n\otimes m} + F^{m\otimes l\otimes n} \\ &\quad + F^{m\otimes n\otimes l} + F^{n\otimes l\otimes m} + F^{n\otimes m\otimes l}). \end{aligned} \tag{15}$$

Additionally, we define the Krylov subspace $K_m(A, p)$ corresponding to matrix A and vector (matrix) p as the space spanned by vectors $\{p, Ap, \ldots, A^{m-1}p\}$.

For the system in (1) and (2), the first-order transfer function for the state-variables x is simply the transfer function of the linearized system

$$(G_1 + sC_1)H_1(s) = b, \quad \text{or} \quad H_1(s) = (G_1 + sC_1)^{-1}b. \tag{16}$$

Defining $\bar{s} = s_1 + s_2$, it can be shown that the second-order transfer function is given by

$$[G_1 + \bar{s}C_1]H_2(s_1, s_2) = -[G_2 + \bar{s}C_2] \cdot \overline{H_1(s_1) \otimes H_1(s_2)} \tag{17}$$

where $\overline{H_1(s_1) \otimes H_1(s_2)} = (1/2)(H_1(s_1) \otimes H_1(s_2) + H_1(s_2) \otimes H_1(s_1))$. Similarly, we define $\overline{H_1(s_1) \otimes H_1(s_2) \otimes H_1(s_3)}$ as the arithmetic average of the terms of all possible permutations of frequency variables in the Kronecker product. With $\tilde{s} = s_1 + s_2 + s_3$, the third-order nonlinear transfer function is given by the following equations:

$$\begin{aligned} &[G_1 + \tilde{s}C_1]H_3(s_1, s_2, s_3) \\ &\quad = -[G_3 + \tilde{s}C_3] \cdot \overline{H_1(s_1) \otimes H_1(s_2) \otimes H_1(s_3)} - 2 \\ &\qquad \cdot [G_2 + \tilde{s}C_2] \cdot \overline{H_1(s_1) \otimes H_2(s_2, s_3)} \end{aligned} \tag{18}$$

$$\begin{aligned} &\overline{H_1(s_1) \otimes H_2(s_2, s_3)} \\ &\quad = \frac{1}{6}\big(H_1(s_1) \otimes H_2(s_2, s_3) + H_1(s_2) \otimes H_2(s_1, s_3) \\ &\qquad + H_1(s_3) \otimes H_2(s_1, s_2) + H_2(s_1, s_2) \otimes H_1(s_3) \\ &\qquad + H_2(s_1, s_3) \otimes H_1(s_2) + H_2(s_2, s_3) \otimes H_1(s_1)\big). \end{aligned} \tag{19}$$

Without loss of generality, we expand (16) at the origin as a Mclaurin series

$$H_1(s) = \sum_{k=0}^{\infty} s^k A^k r_1 = \sum_{k=0}^{\infty} s^k M_{1,k} \tag{20}$$

where $M_{1,k} = A^k r_1$ is the kth-order moment of the first order-transfer function. Expanding $H_2(s_1, s_1)$ at the origin (0, 0), we have

$$H_2(s_1, s_2) = \sum_{k=0}^{\infty} \sum_{l=0}^{k} s_1^l s_2^{k-l} M_{2,k,l} \tag{21}$$

where $M_{2,k,l}$ is a kth-order moment of the second-order transfer function. To derive the expressions for the moments of $H_2(s_1, s_2)$, substituting (20) into (17) and expanding with respect to $\bar{s} = s_1 + s_2$ yields

$$\begin{aligned} H_2(s_1, s_2) &= -(G_1 + \bar{s}C_1)^{-1} \cdot (G_2 + \bar{s}C_2) \cdot \overline{H_1(s_1) \otimes H_1(s_2)} \\ &= -\sum_{m=0}^{\infty} \bar{s}^m A^m G_1^{-1} \cdot (G_2 + \bar{s}C_2) \\ &\quad \cdot \overline{\left(\sum_{k=0}^{\infty} s_1^k M_{1,k}\right) \otimes \left(\sum_{l=0}^{\infty} s_2^l M_{1,l}\right)} \\ &= -\sum_{m=0}^{\infty}\sum_{k=0}^{\infty}\sum_{l=0}^{\infty} \bar{s}^m s_1^k s_2^l A^m G_1^{-1} \\ &\quad \cdot (G_2 + \bar{s}C_2)\overline{A^{k\otimes l}} r_2. \end{aligned} \tag{22}$$

Comparing (21) with (22), we can express the moments of $H_2(s_1, s_2)$ as

$$\begin{aligned} M_{2,k,l} &= -\sum_{p=1}^{k} A^{p-1} \sum_{q=0, q\le l, p-q\le k-l}^{p} \binom{p}{q} \\ &\quad \times G_1^{-1}C_2 \cdot \overline{A^{(l-q)\otimes(k-l-p+q)}} r_2 \\ &\quad - \sum_{p=0}^{k} A^p \sum_{q=0, q\le l, p-q\le k-l}^{p} \binom{p}{q} G_1^{-1}G_2 \\ &\quad \cdot \overline{A^{(l-q)\otimes(k-l-p+q)}} r_2. \end{aligned} \tag{23}$$

TABLE I
MOMENTS OF $H_2(s_1, s_1)$

Order	Moment
0^{th} order	$-G_1^{-1}G_2r_2$
1^{st} order (s_1, s_2 terms)	$-G_1^{-1}C_2r_2 - AG_1^{-1}G_2r_2 - G_1^{-1}G_2\overline{A^{1\otimes 0}}r_2$
2^{nd} order (s_1^2, s_2^2 terms)	$-AG_1^{-1}C_2r_2 - G_1^{-1}C_2\overline{A^{1\otimes 0}}r_2 - A^2G_1^{-1}G_2r_2 - AG_1^{-1}G_2\overline{A^{1\otimes 0}}r_2 - G_1^{-1}G_2\overline{A^{2\otimes 0}}r_2$
2^{nd} order (s_1s_2 term)	$-G_1^{-1}C_2\overline{A^{1\otimes 0}}r_2 - G_1^{-1}G_2\overline{A^{1\otimes 1}}r_2 - AG_1^{-1}G_2\overline{A^{1\otimes 0}}r_2$

Similarly, the third-order transfer function can be expanded at the origin (0, 0, 0) as

$$H_3(s_1,s_2,s_3)=\sum_{k=0}^{\infty}\sum_{l=0}^{k}\sum_{m=0}^{k-l}s_1^l s_2^m s_3^{k-l-m}M_{3,k,l,m} \tag{24}$$

where $M_{3,k,l,m}$ is a kth-order moment given by

$$\begin{aligned}
M_{3,k,l,m}&=-\sum_{p=1}^{k}A^{p-1}\sum_{q=0,q\le l,p-q\le k-l}^{p}\binom{p}{q}\\
&\times\sum_{t=0,t\le m,p-t-q\le k-l-m}^{p-q}\binom{p-q}{t}G_1^{-1}\\
&\times\left[C_3\cdot\overline{A^{(l-q)\otimes(m-t)\otimes(k-l-m-p+q+t)}}r_3+C_2\cdot F\right]\\
&-\sum_{p=0}^{k}A^{p}\sum_{q=0,q\le l,p-q\le k-l}^{p}\binom{p}{q}\\
&\times\sum_{t=0,t\le m,p-t-q\le k-l-m}^{p-q}\binom{p-q}{t}G_1^{-1}\\
&\times\left[G_3\cdot\overline{A^{(l-q)\otimes(m-t)\otimes(k-l-m-p+q+t)}}r_3+G_2\cdot F\right]
\end{aligned} \tag{25}$$

with

$$\begin{aligned}
F=\frac{1}{3}[&(A^{l-q}r)\otimes M_{2,k-l-p+q,m-t}+(A^{m-t}r)\\
&\otimes M_{2,k-m-p+t,l-q}+(A^{k-l-m-p+q+t}r)\\
&\otimes M_{2,l+m-q-t,l-q}+M_{2,k-l-p+q,m-t}\otimes(A^{l-q}r)\\
&+M_{2,k-m-p+t,l-q}\otimes(A^{m-t}r)\\
&+M_{2,l+m-q-t,l-q}\otimes(A^{k-l-m-p+q+t}r)]
\end{aligned} \tag{26}$$

As an example, the first few moments of $H_2(s_1, s_2)$ are shown in Table I. Clearly, nonlinear model order reduction is intrinsically more complex and costly than that of LTI systems. Also note that in (17) and (18), symmetric nonlinear transfer functions (symmetric w.r.t frequency variable permutations) are used. This is advantageous for model reduction as the numbers of moments need to be matched for H_2 and H_3 are approximately reduced by a factor of 2 and 6, respectively, when expanding them at a point with equal coordinates such as the origin.

V. NORM

In this section, the proposed NORM algorithm is presented. For simplicity, we limit our discussion to SIMO time-invariant weakly nonlinear systems. Up to the third-order nonlinear transfer functions are considered in the reduction. Extension to more general periodically time-varying systems is presented in the Appendix (Section VIII-B). To assess the model order-reduction quality from a moment-matching perspective, we first have the following definition.

Definition 1: A nonlinear reduced order model is a kth-order model in $H_1(s)$ ($H_2(s_1, s_2)$ or $H_3(s_1, s_2, s_3)$) if and only if up to kth-order moments $M_{1,l}, 0 \le l \le k$, ($M_{2,l,m}, 0 \le l \le k, 0 \le m \le l$ or $M_{3,l,m,n}, 0 \le l \le k, 0 \le m \le l, 0 \le n \le l - m$) of the first (second- or third-order) transfer function of the original system defined in (20), ((21), or (24)) are preserved in the reduced model.

According to Definition 1, a second-order reduced model in H_2 preserves the moments of H_2 which correspond to the coefficients of terms $s_1^0(s_2^0), s_1, s_2, s_1s_2, s_1^2$ and s_2^2 in the expansion.

A. Single-Point Expansion

To derive a set of minimum Krylov subspaces for the most compact order reduction, understanding the interaction between the moments of nonlinear transfer functions at different orders is important. For the moment matching of $H_2(s_1, s_2)$, this interaction is manifested in (22). The $s_1^p s_2^q$ term in the expansion of H_2, where p, q are integers, is a consequence of two power series expansions: expansion of H_1 in (20) and that of H_2 in (22) with respect to $\bar{s} = s_1 + s_2$. As a result, the kth-order moment of H_2 depends on the moments of H_1 with an order less or equal to k. As such, the final expression for $M_{2,l,m}$ is in a form as shown in (23). The expression for $M_{3,l,m,n}$ is derived similarly in a more complex form in (25).

If we were to use a projection for order reduction, the key issue would be to find certain Krylov subspaces, which contain all the moments to be matched. To minimize the number of projection vectors needed, nonlinear transfer function moments have to be considered explicitly. A close inspection of (23) reveals that the Krylov subspaces of matrix A given in Table II are the desired Krylov subspaces of the minimum total dimension for constructing a kth-order model in H_2. For the last row, $m = \lfloor k/2 \rfloor, n = k - \lfloor k/2 \rfloor, p = \lfloor (k-1)/2 \rfloor$, and $q = k - 1 - \lfloor (k-1)/2 \rfloor$. We denote the union of Krylov subspaces in Table II as $K2(k) = \cup_i K_{m_i}(A, v_i)$, where k in the

TABLE II
KRYLOV SUBSPACES SPANNED BY MOMENTS OF H_2

Starting vector v_i	Subspace Dim m_i	Starting vector v_i	Subspace Dim m_i
$G_1^{-1}G_2\overline{A^{0\otimes 0}}r_2$	$k+1$	$G_1^{-1}C_2\overline{A^{0\otimes 0}}r_2$	k
$G_1^{-1}G_2\overline{A^{1\otimes 0}}r_2$	k	$G_1^{-1}C_2\overline{A^{1\otimes 0}}r_2$	$k-1$
...	...	...	...
$G_1^{-1}G_2\overline{A^{k\otimes 0}}r_2$	1	$G_1^{-1}C_2\overline{A^{(k-1)\otimes 0}}r_2$	1
$G_1^{-1}G_2\overline{A^{1\otimes 1}}r_2$	$k-1$	$G_1^{-1}C_2\overline{A^{1\otimes 1}}r_2$	$k-2$
$G_1^{-1}G_2\overline{A^{2\otimes 1}}r_2$	$k-2$	$G_1^{-1}C_2\overline{A^{2\otimes 1}}r_2$	$k-3$
...	...	...	...
$G_1^{-1}G_2\overline{A^{(k-1)\otimes 1}}r_2$	1	$G_1^{-1}C_2\overline{A^{(k-2)\otimes 1}}r_2$	1
...	...	...	...
$G_1^{-1}G_2\overline{A^{m\otimes n}}r_2$	1	$G_1^{-1}C_2\overline{A^{q\otimes p}}r_2$	1

parenthesis indicates the order of H_2 moments up to which contained in the subspaces. In an analogous and somewhat more involved way, a set of minimum Krylov subspaces $K3(k)$ for the moment-matching of H_3 up to kth order can also be derived. More specifically, (25) and (26) show that the required subspace $K3(k) = \cup_i K_{m_i}(A, v_i)$ consists of a collection of Krylov subspaces of A, where the starting vector v_i takes one of the following forms:

$$G_1^{-1}G_3\overline{A^{l\otimes m\otimes n}}r_3, \quad G_1^{-1}C_3\overline{A^{l\otimes m\otimes n}}r_3,$$
$$G_1^{-1}G_2\overline{(A^l r_1)\otimes M_{2,(m,n)}}, \quad \text{or} \quad G_1^{-1}C_2\overline{(A^l r_1)\otimes M_{2,(m,n)}} \tag{27}$$

with

$$\begin{aligned}\overline{(A^l r)\otimes M_{2(m,n)}} &= \frac{1}{3}\big((A^l r_1)\otimes M_{2,m+n,n} + (A^m r_1)\otimes M_{2,l+n,n} \\ &\quad + (A^n r_1)\otimes M_{2,l+m,l} + M_{2,m+n,n}\otimes(A^l r_1) \\ &\quad + M_{2,l+n,n}\otimes(A^m r_1) + M_{2,l+m,l}\otimes(A^n r_1)\big).\end{aligned} \tag{28}$$

Using these subspaces we can rigorously prove the following theorem.

Theorem 1: Let V is an orthonormal basis for the union of subspaces $K_{k_1+1}(A, r_1), K2(k_2)$, and $K3(k_3)$, where $k_1 \geq k_2 \geq k_3$. Then, the reduced order model specified by the following system matrices:

$$\begin{aligned}&\tilde{G}_1 = V^T G_1 V, \quad \tilde{C}_1 = V^T C_1 V, \quad \tilde{b} = V^T b, \quad \tilde{D} = V^T D \\ &\tilde{G}_2 = V^T G_2(V\otimes V), \quad \tilde{C}_2 = V^T C_2(V\otimes V), \\ &\tilde{G}_3 = V^T G_3(V\otimes V\otimes V), \quad \tilde{C}_3 = V^T C_3(V\otimes V\otimes V)\end{aligned} \tag{29}$$

is a k_1th-order model in H_1, a k_2th-order model in H_2 and a k_3th-order model in H_3 for the nonlinear system of (1) or (2) if $\tilde{G}_1$ defined above is full-rank. Namely,

$$M_{1,l} = V\cdot\tilde{M}_{1,l} \quad \text{for all } 0 \leq l \leq k_1 \tag{30}$$
$$M_{2,l,m} = V\cdot\tilde{M}_{2,l,m} \quad \text{for all } 0 \leq l \leq k_2, \quad 0 \leq m \leq l. \tag{31}$$

Input: $G_1, C_1, G_2, C_2, G_3, C_3, b, D, k_1, k_2, k_3, k_1 \geq k_2 \geq k_3$

1. Compute a Krylov subspace of A to match up to k_1-th order moments of H_1: $V_1 \leftarrow qr(K_{k_1+1}(A, r_1))$.
2. Compute the following Krylov subspaces to match the moments of H_2 up to k_2-th order: $V_2 \leftarrow [\ ]$;
   2.1. For each $m \geq 0, n \geq 0, m \leq n, m+n \leq k_2$:
   $v = G_1^{-1}G_2\overline{A^{m\otimes n}}r_2$, $V_2 \leftarrow [V_2, qr(K_{k_2-m-n+1}(A, v))]$
   2.2. For each $m \geq 0, n \geq 0, m \leq n, m+n \leq k_2-1$:
   $v = G_1^{-1}C_2\overline{A^{m\otimes n}}r_2$, $V_2 \leftarrow [V_2, qr(K_{k_2-m-n}(A, v))]$
3. To match the moments of H_3 up to k_3-th order compute the following Krylov spaces: $V_3 \leftarrow [\ ]$;
   3.1. For each $m \geq 0, n \geq 0, l \geq 0, m \leq n \leq l, m+n+l \leq k_3$:
   $v = G_1^{-1}G_3\overline{A^{l\otimes m\otimes n}}r_3$, $V_3 \leftarrow [V_3, qr(K_{k_3-m-n-l+1}(A, v))]$
   $v = G_1^{-1}G_2\overline{(A^l r_1)\otimes M_{2,(m,n)}}$, $V_3 \leftarrow [V_3, qr(K_{k_3-m-n-l+1}(A, v))]$
   3.2. For each $m \geq 0, n \geq 0, l \geq 0, m \leq n \leq l, m+n+l \leq k_3-1$:
   $v = G_1^{-1}C_3\overline{A^{l\otimes m\otimes n}}r_3$, $V_3 \leftarrow [V_3, qr(K_{k_3-m-n-l}(A, v))]$
   $v = G_1^{-1}C_2\overline{(A^l r_1)\otimes M_{2,(m,n)}}$, $V_3 \leftarrow [V_3, qr(K_{k_3-m-n-l}(A, v))]$
4. $V = qr([V_1, V_2, V_3])$, $\tilde{G}_1 = V^T G_1 V$, $\tilde{C}_1 = V^T C_1 V$, $\tilde{b} = V^T b$, $\tilde{D} = V^T D$, $\tilde{G}_2 = V^T G_2(V\otimes V)$, $\tilde{C}_2 = V^T C_2(V\otimes V)$, $\tilde{G}_3 = V^T G_3(V\otimes V\otimes V)$, $\tilde{C}_3 = V^T C_3(V\otimes V\otimes V)$.

Fig. 2. Single-point NORM algorithm.

$$M_{3,l,m,n} = V\cdot\tilde{M}_{3,l,m,n}$$
$$\text{for all } 0 \leq l \leq k_3, \quad 0 \leq m \leq l, \quad 0 \leq n \leq l-m \tag{32}$$

where $\tilde{M}_{1,l}, \tilde{M}_{2,l,m}$, and $\tilde{M}_{3,l,m,n}$ are the moments of the reduced order model.

A proof of the theorem can be found in Section A of the Appendix. The complete single-point version of NORM algorithm (expanded at the origin) is shown in Fig. 2, where $\mathrm{qr}(\cdot)$ indicates the QR procedure used for othonormalizing the input vectors. It should be noted that the Kronecker product form of the starting vectors of the required Krylov subspace involves power terms of matrix A. This means that a direct computation of starting vectors which depend on high order power terms of A might not be numerically stable due to the machine round off errors. A remedy to this problem for reducing H_2 is to employ orthogonalization both within each individual Krylov subspace and between starting vectors of different Krylov subspaces. A similar stable orthogonalization procedure can be applied for the reduction of H_3, however, with an increase in the size of the reduced model. Nevertheless, as will be demonstrated in the circuit examples, due to the model size limitation on nonlinear model reduction, only a low-order moment-matching (e.g., <6th order) is feasible in practice. Therefore, numerical instability is usually not an issue compared to the compactness of the reduced-order model. This potential numerical instability can be also ameliorated by using a multipoint approach as presented later on in this paper which further improves the model compactness.

Also note that in Fig. 2, to compute any Kronecker product term, one can exploit the original problem sparsity such that the computation takes only a linear time in the problem size. The requirement $k_1 \geq k_2 \geq k_3$ is due to the dependence of high-order nonlinear transfer functions on transfer functions of lower orders. Provided this condition is satisfied, the order of moment matching for each nonlinear transfer function can be flexibly chosen to fit specific needs. For each of these choices, a reduced-order model of minimum size is produced as described in the following section. It is worth mentioning that a singular calue decomposition (SVD) step is commonly used to remove the redundancy in the projection subspace prior to constructing the final model as in Step 4 of Fig. 2. However, redundant projection vectors that do not contribute to the moment matching introduced by the technique in [8], [10] may not be removed by this numerical procedure. The reason is simply that these redundant vectors are not necessarily linearly independent of the useful ones.

B. Size of Reduced-Order Models

Similar to the linear case, we define the size of a nonlinear model as shown in (2) in terms of its number of unknowns. Under the context of projection-based framework, the size of a nonlinear reduced-order model is equal to the total number of projection vectors employed to approximate nonlinear transfer functions of different orders. Consider the size of the SIMO-based reduced-order models generated using the method of [8], [10] under Definition 1. It can be shown that if the linear networks described by (10)–(12) are each reduced to a system preserving up to k_1, k_2, and k_3th-order moments of the original system, respectively, then the overall reduced nonlinear model is a k_1th-order model in H_1, a $\overline{k_2}$th-order model in H_2, where $\overline{k_2} = \min(k_1, k_2)$ and a $\overline{k_3}$th-order model in H_3, where $\overline{k_3} = \min(k_1, k_2, k_3)$. For instance, from (22), the final moment expressions of H_2 are a consequence of expanding with respect to s in (20) and expanding with respect to $\bar{s}$ in (22). Therefore, the lesser of k_1 and k_2 determines the order up to which the moments of $H_2(s_1, s_2)$ are matched. This reveals that for the method in [8]and [10], the most compact kth-order model in H_2 with a size in $O(k^3)$ is achieved by choosing $k_1 = k_2 = k$. In other words, choosing $k_2 > k_1 = k$ does not necessarily increase the number of moments of H_2 matched in the reduced model. On the other hand, if one would like to have $k_1 > k_2$ to increase the accuracy in H_1, the best way is to only make use of the first $k_2 + 1$ moment directions of H_1 when reducing H_2, while the remaining H_1 moments are included in the projection only for matching H_1 itself. Similarly, for the method in [8] and [10], the optimal way to generate a kth-order model in H_3 is to choose $k_1 = k_2 = k_3 = k$ with a resulting model size of $O(k^5)$. Note that these strategies are also employed in the single-point NORM algorithm. To compare with the above "optimal" model sizes achievable from the method of [8] and [10], in single-point NORM the sizes of a kth-order model in H_2 and H_3 are in $O(k^3)$ and $O(k^4)$, respectively. This can be seen by counting the total dimensions of the Krylov subspaces used in Fig. 2. The exact model sizes for several values of k will be shown in the following section.

C. Multipoint Expansions

To target at a system's particular input-frequency band of interest, particularly for RF circuits, it might be desirable to expand both linear and nonlinear transfer functions at points other than the origin, such as along the imaginary axis. It is crucial to note that under the nonlinear context, a single-frequency expansion point along the imaginary axis may inherit multiple matrix factorizations due to the nonlinear frequency mixing effects. To this end, suppose that the in-band third-order intermodulation of a nonlinear system around center frequency f_0 is important to model. To build the most compact model, one would opt to expand $H_1(s)$ at $s = j2\pi f_0$. To correctly perform moment matching for H_2 and H_3, the respective expansion points for high-order transfer functions should be $(j2\pi f_0, j2\pi f_0)$ and $(j2\pi f_0, -j2\pi f_0)$ for H_2, and $(j2\pi f_0, j2\pi f_0, -j2\pi f_0)$ for H_3, respectively. Here, the use of two expansion points for H_2 takes care of matching second order mixing effects in terms of both sum and difference frequencies around the center frequency, and also ensures the moment matching of the third-order in-band intermodulations. These choices of expansion points require the system matrix factorized at dc and $j4\pi f_0$ in addition to $j2\pi f_0$ in (11)–(12) or (17)–(18). Therefore, if every linear system in (10)–(12) is reduced by expanding at $s = j2\pi f_0$ using the method of [8] and [10], then the intended moment directions of H_2 and H_3 are not guaranteed to be matched. Instead, some other subspace vectors, which are usually not the most desirable, might be preserved in the reduced order model.

In addition to the benefit of using specific expansion points, a multipoint projection, where several expansion points are used simultaneously, has a unique efficiency advantage in terms of model compactness over the single-point method. Although multipoint methods do not bring such an advantage for LTI system reduction, adopting multipoint methods for nonliner systems can lead to significantly smaller reduced models. To see this, first notice the unsurprising fact that the size of the nonlinear reduced order model grows faster than the order of moment matching. This stems from the fact that as the order of moment matching proceeds, significantly more moments corresponding to various expansion terms emerge for multivariable high-order transfer functions. However, it is much more revealing to recognize that the numbers of up to k-th-order moments of H_2 and H_3 are $k(k+1)/2$ and $O(k^3)$, respectively, therefore, the dimension of the subspaces used in the projection grows even faster than the number of moments matched in the single-point expansion version of NORM.[1] This is because matching a high-order moment of a nonlinear transfer function would in general require the use of more than one projection vector. In contrast, to preserve the value of a nonlinear transfer function at a specific point (a zeroth-order moment), only one vector needs to be included in the projection, assuming that the dependency between transfer functions of different orders is resolved properly. In other words, the reduced model size of a zeroth-order multipoint method is the same as the number of moments matched. For the expanded MNA formulation in (2),

[1]Using the bilinear form can produce models with a size proportional to number of moments matched, however, this may be offset by the inflated problem size and the accuracy degradation for reducing a significantly larger system.

TABLE III
COMPARISON ON THE REDUCED ORDER MODEL SIZES

Order K	3	4	5	6	7	8	9
[8][10]: H_1-H_2	116	230	402	644	968	1,386	1,910
NORM-sp: H_1-H_2	24	40	62	91	128	174	230
NORM-mp: H_1-H_2	14	20	27	35	44	54	65
[8][10]: H_1-H_2-H_3	3,700	11,480	28,914	63,070	123,848	224,460	381,910
NORM-sp: H_1-H_2-H_3	66	118	194	301	446	636	880
NORM-mp: H_1-H_2-H_3	34	55	83	119	164	219	285

we compare the worst-case reduced-order model sizes generated by three methods, the method of [8] and [10], single-point NORM and multipoint NORM in Table III, where two different cases are considered.[2] In the first case, we consider the size of a kth-order model in H_1 and H_2 for various values of k, i.e., the reduced-order model matches the moments of both transfer functions up to order k. In the second case, we consider the size of a kth-order model in H_1, H_2, and H_3. To count the size of a model (number of unknowns), we sum up the total number of projection vectors employed to preserve the moments of all the transfer functions considered. In the table, the "optimal" strategies outlined in the previous section are used for the method of [8], [10]. NORM-sp denotes the single-point based NORM. For these two methods, the expansion point is assumed to be the origin. In Table III, NORM-mp is the "equivalent" zeroth-order multipoint method that preserves the same number of moments as resulted by expanding all the transfer functions considered to kth order at an arbitrary expansion point.[3] As clearly shown, using NORM, the model compactness can be significantly improved.

With respect to the circuit size, single-point and multipoint NORM both have a near-linear complexity for typical sparse circuit problems since the dominant computational cost is due to the linear system solution(s). Given the same model size, multipoint methods are more expansive than single-point methods due to the additional matrix factorizations. In a multipoint approach, where low-order moment-matchig is performed at several expansion points, the computational cost incurred by more than one matrix factorizations might be alleviated by exploiting the idea of recycled Krylov-subspace vectors for time-varying systems [15], [17]. It is also possible to use constant Jacobian iterations to iteratively solve the resulted linear problems for narrow band systems, such as certain RF applications. The LU factorization at one expansion point might be reused as an approximated Jacobian for another point that is not far away in the iteration [20]. One additional advantage of multipoint methods is that they help to eliminate the potential numerical stability problem of the single-point methods for high order moment matching.

D. Results

We compared the method of [8] and [10], single-point NORM (NORM-sp) and zeroth-order multipoint NORM (NORM-mp) on several examples. For the first two methods, the origin was chosen as the expansion point. Note that the optimal strategies presented in Section V-B were applied to the method in [8] and [10], otherwise, significantly larger models would result with little accuracy improvement. For all three methods, an SVD procedure follows the computation of Krylov subspace vectors to deflate the subspaces as much as possible.

1) Diode Circuit: We first consider the diode circuit in Fig. 3(a), which is similar to the example studied in [21], but with one inductor added to each diode/resistor/capacitor stage. To compare different methods, we created a 751 state variable problem by adding 250 stages. The input is a small-signal current source, and the output is the capacitor voltage at the last stage. Each diode's nonlinear I-V characteristics is modeled using a second order polynomial at the bias point. The method of [8] and [10] generates a model of 45 states matching five moments of H_1, two moments of both H_2 and H_3. NORM-sp matches five moments of H_1, nine moments of H_2, four moments of H_3, resulting a reduced model with 23 states. NORM-mp produces a model with 18 states while matching five moments of H_1, ten moments of H_2, and four moments of H_3. As can be seen, NORM is able to generate smaller model while matching more moments due to its improved selection of Krylov subspace vectors. The second-order transfer function $H_2(j2\pi f_1, j2\pi f_2)$, where $0 \leq f_1, f_2 \leq 50$ MHz is plotted based on full model and three reduced models in Fig. 3. The maximum relative errors of the method of [8], [10], NORM-sp and NORM-mp are about 0.35%, 0.06%, and 0.011%, respectively. For our harmonic balance simulations, we applied a 5 MHz sinusoidal input with a 1-mV magnitude to various models. The reduced models due to [8], [10], NORM-sp and NORM-mp led to a runtime speedup of $41\times, 118\times$, and $189\times$ over the full model, respectively, in a harmonic balance simulator implemented in MATLAB.

2) Double-Balanced RF Mixer: For more realistic examples, next, we consider a standard double-balanced mixer in Fig. 4, modeled as a periodically time-varying weakly nonlinear system. Circuit nonlinearities are modeled using third order polynomials around the time-varying operating point due to the large local oscillator (LO) signal. The full model has 2403 time-sampled circuit unknowns and is characterized by periodically time-varying Volterra series. The 60 state model generated by the method of [8], [10] matches 4 moments of H_1, 2 moments of both H_2 and H_3. NORM-sp generates a model with 19 states matching four moments for all of H_1, H_2, and H_3. NORM-mp matches 4 moments of H_1 and H_3, 8 moments of algorithms were implemented using C++ and executed on an IBM RS6000H_2 resulting a model size of 14. The three

[2]The model sizes given in [18] and [19] are somewhat different. The corrected values are shown in Table III.

[3]To count the total number of up to kth-order moments, we assume the expansion point is arbitrary. Special expansion points such as the origin will lead to a less number of nonlinear transfer function moments.

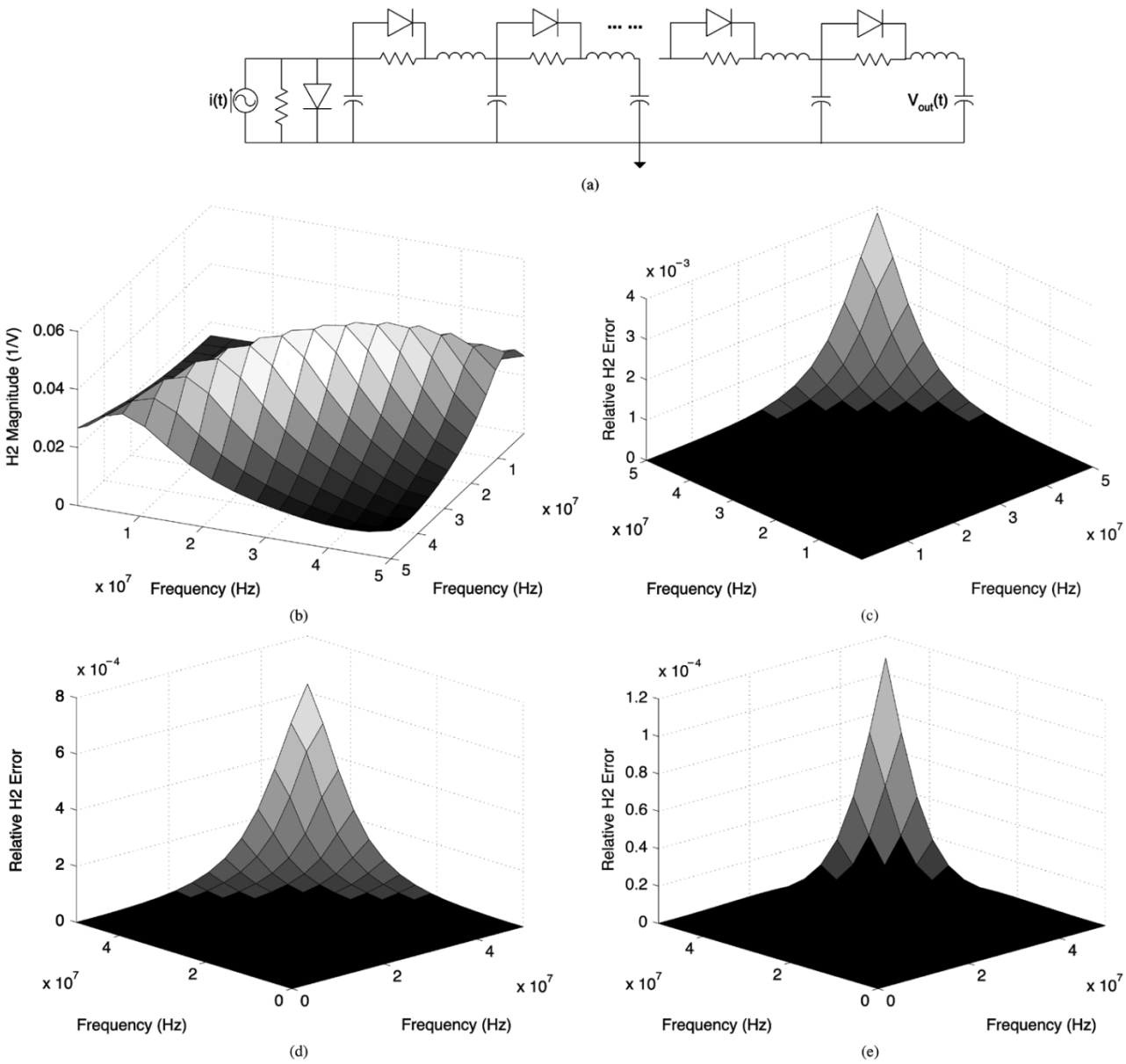

Fig. 3. (a) Diode circuit. (b) Original H_2 (751 states). (c) Relative error of the method of [8] and [10] (45 states). (d) Relative error of NORM-sp (23 states). (e) Relative error of NORM-mp (18 states).

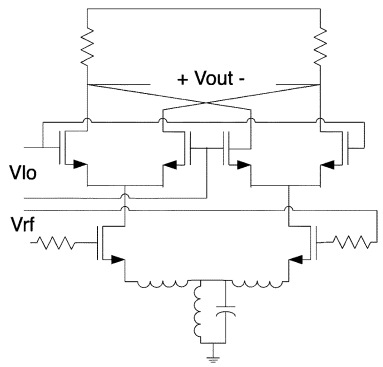

Fig. 4. Double-balanced RF mixer.

nonlinear model reduction workstation. It took 641, 12, and 5 CPU seconds to compute the reduced order models for the method in [8], [10], NORM-sp and NORM-mp, respectively. For this circuit example, the model generation runtime was dominated by the time spent on forming the large and dense third order matrices. As a result, it took less time to generate the 14-state model of NORM-mp than the 19-state model of NORM-sp even though more matrix factorizations were performed in the former. Since the double-balanced mixer is fully symmetric, the second order transfer function H_2 is ideally zero (except for numerical noise). To see the third order intermodulation translated by one LO frequency, the corresponding harmonic of the third order periodically time-varying nonliner transfer function $H_3(t, j2\pi f_1, j2\pi f_2, j2\pi f_3)$ where 100 MHz $\leq f_1, f_2 \leq$ 1.5 GHz, $f_3 = 900$ MHz is plotted in Fig. 5. The maximum relative errors are 27%, 13%, and 4.5%, respectively, for the method of [8] and [10], NORM-sp, and NORM-mp. These models were also simulated for two-tone third-order intermodulation tests using a prototyped harmonic-balance simulator implemented in MATLAB. We first fixed the RF

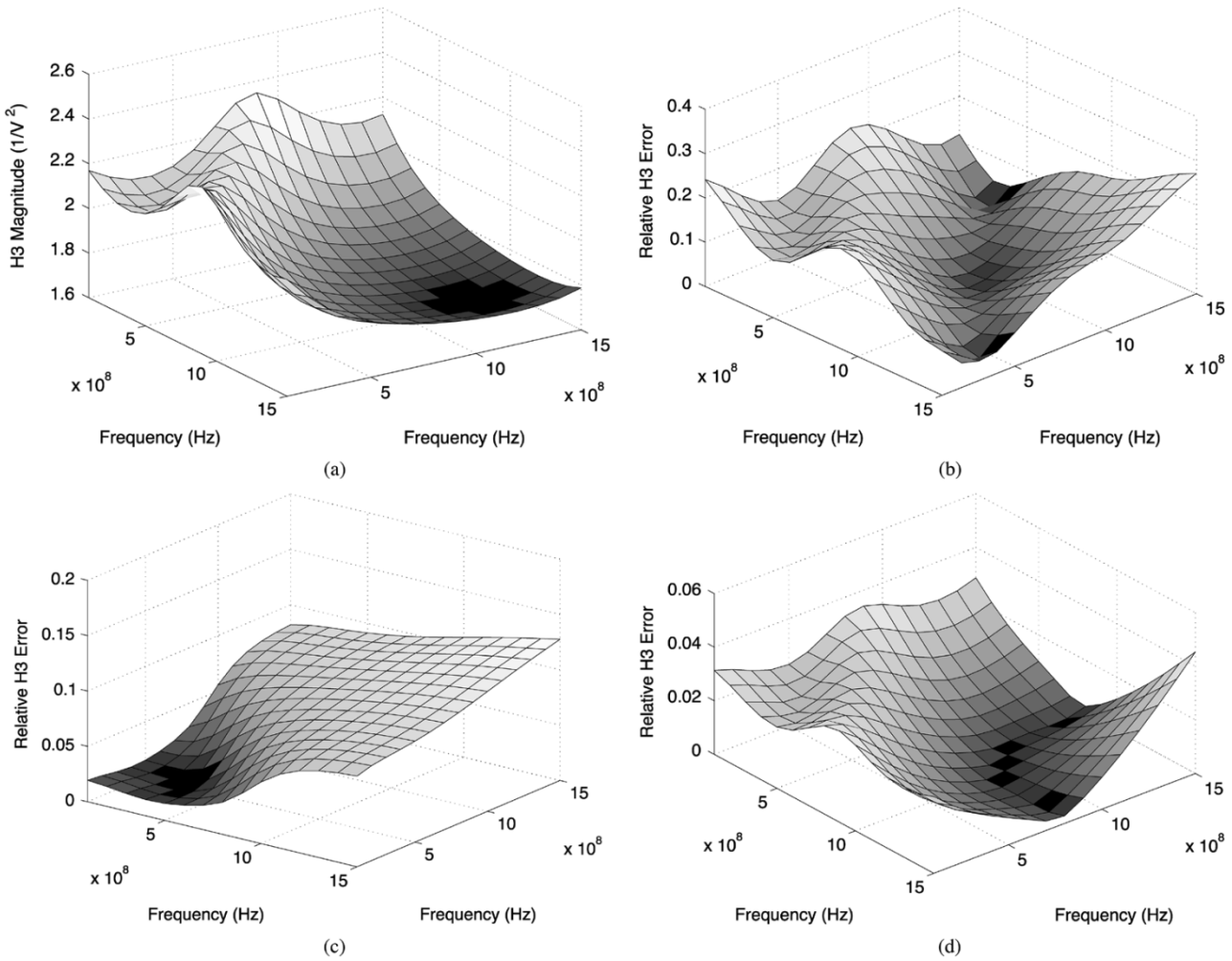

Fig. 5. (a) Original H_3 (2403 unknowns). (b) Relative error of the method of [8], [10] (60 states). (c) Relative error of NORM-sp (19 states). (d) Relative error of NORM-mp (14 states).

input amplitude for both tones at 40 mV, while varying the frequency of one tone from 100 MHz to 2 GHz (the second tone was separated from the first one by 800 kHz). Then, we fixed two tone frequencies at 600 and 600.8 MHz, respectively, but varied the amplitude of the two tones from 20 to 70 mV. The simulation results are plotted in Fig. 6. As can be seen from Fig. 6, the model generated by NORM-mp is the most accurate and also the smallest one for both cases. The 60-state model generated by the method of [8] and [10] incurs apparent error for the first test. Also note that the amount of IM3 (third-order intermodulation) from the simulation is well predicted by the corresponding third-order transfer functions.

Simultation runtimes are summarized in Table IV. Due to the large size of resulting third-order matrices, the 60-state model of the method of [8] and [10] brought less than five times runtime speedup over the full model. However, the much smaller models produced by NORM-sp and NORM-mp brought significant runtime speedups, respectively.

3) 2.4-GHz Subharmonic Direct-Conversion Mixer: A 2.4-GHz subharmonic direct-conversion mixer used in WCDMA applications is shown in Fig. 7. It employs six phases of an LO signal at 800 MHz to generate an equivalent LO at 2.4 GHz. For direct-conversion mixers, second-order nonlinear effects are important, which exist when the perfect circuit symmetry is lost in a balanced architecture. For this example, we introduced about 2% transistor width mismatch in the circuit and applied the three methods to reduce the original periodically time-varying system with 4130 time-sampled circuit unknowns. Each circuit nonlinearity is modeled using a periodically time-varying third order polynomial. The zeroth-order harmonic of the time-varying H_2 specifying the mixing of two RF tones directly to the baseband is examined, where, two RF frequencies vary from -2.6 to $-$ 2.2 GHz, and from 2.2 to 2.6 GHz, respectively. The model produced by the method of [8] and [10] has 122 states and matches four moments of H_1, six moments of H_2, and two moments of H_3 with the maximum relative error about 700% or 16.9 dB. NORM-sp produces a model with 34 states while matching five moments of H_1, nine moments of H_2, and two moments of H_3. The maximum relative error for this model is about 14%. For both methods, the origin was used as the expansion point. The better accuracy obtained in the smaller model of NORM-sp can be explained by the fact that a larger number of moments are matched in the reduced model. We anticipate that both methods will generate more accurate models when the correct procedure is employed to expand transfer functions at a

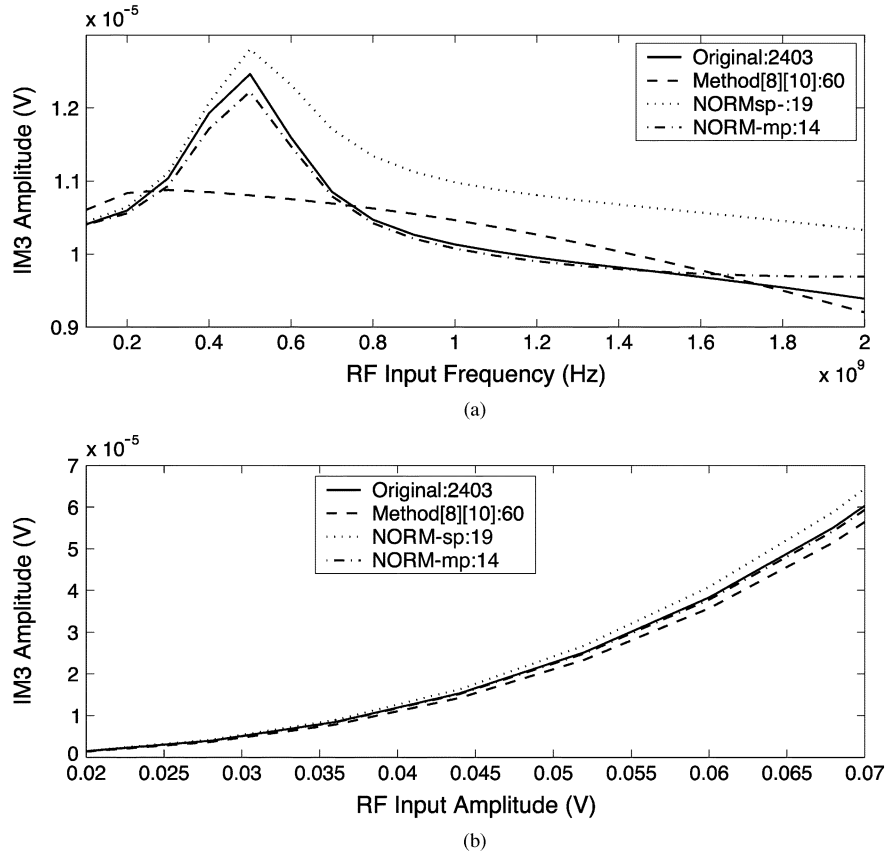

Fig. 6. (a) IM3 as a function of input frequency. (b) IM3 as a function of input amplitude.

TABLE IV
RUNTIME COMPARISON OF THE THREE METHODS ON THE RF MIXER

Model	Full	[8][10]	NORM-sp	NORM-mp
Size	2403	60	19	14
CPU Time (sec.) Sweeping Frequency	827~911	238~247	2.22~2.52	1.14~1.18
CPU Time (sec.) Sweeping Amplitude	420~1,072	107~299	1.06~2.81	0.57~1.28

point close to the center frequency as outlined in Section V-C. Lastly, NORM-mp generates a compact 22-state model with the smallest maximum relative error of 4% while matching six moments of H_1, 12 moments of H_2 and four moments of H_3. The corresponding H_2 harmonic of the full model, those of reduced model due to NORM-mp and NORM-sp are shown in Fig. 8. Executed on an IBM RS6000 workstation, it took 17 and 14 CPU s to compute the projection matrix and form the reduced first and second order matrices for the 34-state model of NORM-sp and the 22-state model of NORM-mp, respectively. In a two-tone harmonic balance simulation in MATLAB, we applied two RF sinusoidal tones around 2.4 GHz with 2 mV amplitude. The simulation based on the full model took about 2417 s to complete while explicitly formed reduced models of NORM-sp and NORM-mp reduced the CPU time to 11.5 and 2.3 s, respectively. Due to the large reduced high-order system matrices, however, it becomes expensive to use the explicitly formed 122-state model of the methods of [8] and [10]. Only the projection matrix was used to reduce the size of the linear problem solved at each simulation iteration. Consequently, the corresponding model did not provide a significant runtime speedup.

VI. HYBRID APPROACH

Many circuits in RF and analog signal processing applications have sharp frequency selectivity (e.g., containing high-Q filtering). For these cases, as the nonlinear frequency-domain system characteristics may vary dramatically within the band of interest, a full projection-based reduction often requires the use of a significant number of projection vectors for achieving sufficient accuracy. As a consequence, forming reduced high-order system matrices can be very expensive due to the large reduced-order model size. Therefore, other types of model simplification are needed. Although numerous nonlinearities can exist in a circuit, there is often a natural tendency for only a few of them to be dominant due to the specific circuit structure. Thus, identifying these dominant nonlinearities within the original circuit structure can be a very useful component of model generation. In the proposed hybrid approach, to cope with stiff circuit problems such as high-Q circuits, the low-order (first and second) responses are matched using projection, while high-order (third) response are approximated by exploiting both the circuit internal structure and projection-based model order reduction.

A. Approximation of Low-Order Responses

For the hybrid approach, we consider the more general scenario of the periodically time-varying weakly nonlinear

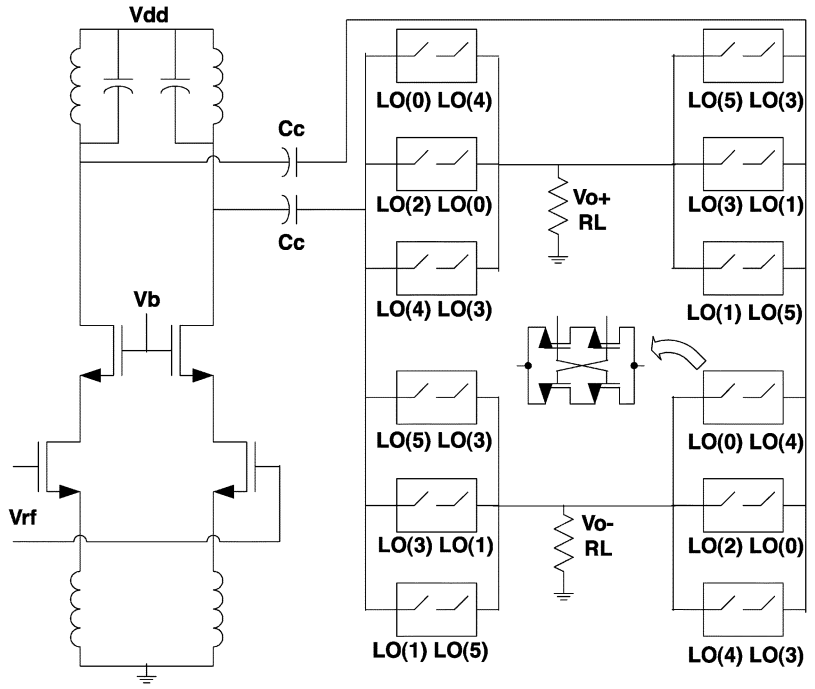

Fig. 7. 2.4-GHz subharmonic direct-conversion mixer.

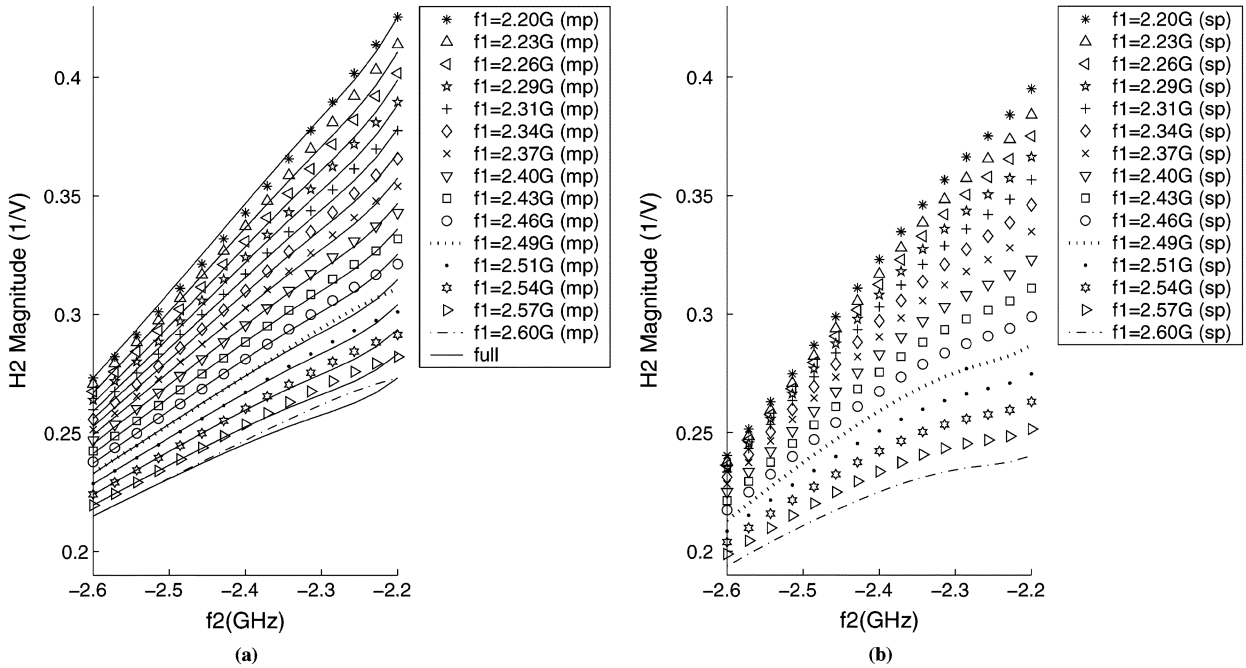

Fig. 8. (a) H_2 of the full model (4130 unknowns) and that of the reduced model due to NORM-mp (22 states). Each reduced model curve is shown in a patterned line and the corresponding one of the full model is the nearest solid line. (b) H_2 of the reduced model due to NORM-sp (34 states). H_2 of the full model is not shown.

systems. Instead of using a time-invariant Volterra description, these systems can be characterized by periodically time-varying nonlinear transfer functions $H_n(t,\cdot)$. As discussed in Section B of the Appendix, $H_n(t,\cdot)$ can be discretized using backward-Euler rule based on M sample points $\overline{H_n} = [H_n(t_1,\cdot)^T, H_n(t_2,\cdot)^T, \ldots, H_n(t_M,\cdot)^T]^T$ within a period of the system time variation T. Analogous to the use of $G_1, C_1, b_1, G_2, C_2, G_3, C_3$ in (16)–(18), a set of matrices $\overline{G_1}, \overline{C_1}, \overline{b_1}, \overline{G_2}, \overline{C_2}, \overline{G_3}, \overline{C_3}$ can be formulated based on the discretization of the system nonlinear characteristics over a period of T for periodically time-varying systems. Using these matrices, (16)–(18) can be reformulated in terms of $\overline{H_1}, \overline{H_2}, \overline{H_3}$. Each of these equations now has $M \times N$ unknowns and can be reduced directly using NORM, where N is the number of physical circuit unknowns of the system.

Assume that $M = 2K - 1$, where, K is an integer, and consider the application of NORM algorithm to approximate the first and second nonlinear transfer functions. We denote the

corresponding projection matrix as $V \in R^{NM\times q}$, where q is the size of reduced order model. We further denote the reduced first and second order matrices produced by NORM as

$$\begin{aligned}\tilde{G}_1 &= V^T\overline{G_1}V \in R^{q\times q}\\ \tilde{C}_1 &= V^T\overline{C_1}V \in R^{q\times q}\\ \tilde{b} &= V^T\overline{b} \in R^{q\times 1}\\ \tilde{G}_2 &= V^T\overline{G_2}(V\otimes V) \in R^{q\times q^2}\\ \tilde{C}_2 &= V^T\overline{C_2}(V\times V) \in R^{q\times q^2}.\end{aligned} \tag{33}$$

Substituting (33) into (16) and (17), the first- and second-order transfer functions $\tilde{H}_1$ and $\tilde{H}_2$ of the reduced model can be computed. The time-sampled first- and second-order transfer functions of the original system can be approximated as

$$\widehat{\overline{H_1}} = V\tilde{H}_1, \widehat{\overline{H_2}} = V\tilde{H}_2. \tag{34}$$

As the reduced model of (33) and (34) represents a time-invariant system, the approximation of the first- and second-order responses of the original periodically time-varying system involves the use of discrete Fourier transform. It can be shown that the following qth-order system is a time-domain realization of the corresponding reduced model

$$\begin{cases}\dfrac{d}{dt}(\tilde{C}_1\tilde{x}_1)+\tilde{G}_1\tilde{x}_1 = \tilde{b}u_s(t)\\ \dfrac{d}{dt}(\tilde{C}_1\tilde{x}_2)+\tilde{G}_1\tilde{x}_2 = \dfrac{d}{dt}(\tilde{C}_2(\tilde{x}_1\otimes\tilde{x}_1))-\tilde{G}_2(\tilde{x}_1\otimes\tilde{x}_1)\\ \tilde{y}(t)=\begin{bmatrix}\tilde{y}_1\\ \tilde{y}_2\end{bmatrix}=\begin{bmatrix}J & 0\\ 0 & J\end{bmatrix}\begin{bmatrix}\tilde{x}_1\\ \tilde{x}_2\end{bmatrix}\end{cases} \tag{35}$$

where $J = D\cdot\Gamma\cdot V, \Gamma$ is the DFT matrix converting M time samples to the corresponding Fourier coefficients, $D = [e^{-jK\omega_0 t}I_{N\times N},\ldots,I_{N\times N},\ldots,e^{jK\omega_0 t}I_{N\times N}], I_{N\times N}$ is the $N\times N$ identity matrix. The first- and second-order responses of the original system can be approximated in time-domain by $\hat{x}_1=\tilde{y}_1, \hat{x}_2=\tilde{y}_2$.

B. Approximation of the Third-Order Response

In a full projection-based approach, nonlinear model order reduction can be limited by the difficulty in explicitly forming the projected (dense) third-order system matrices, especially for relatively large model size. In this section, we show that pruning-based model simplification can be instead performed in the original system coordinates. Thus, the sparsity of the original circuit problem is not lost, but further enhanced. To approximate the third-order transfer function based on the reduced model of (33) and (34) or (35), substitute (33) into (18)

$$[\overline{G_1}+\tilde{s}\overline{C_1}]\widehat{\overline{H_3}}(s_1,s_2,s_3) = g \tag{36}$$

where

$$\begin{aligned}g &= [\overline{G_3}+\tilde{s}\overline{C_3}]\cdot u_1 + [\overline{G_2}+\tilde{s}\overline{C_2}]\cdot u_2\\ u_1 &= -\overline{\big(V\tilde{H}_1(s_1)\big)\otimes\big(V\tilde{H}_1(s_2)\big)\otimes\big(V\tilde{H}_1(s_3)\big)}\\ u_2 &= -2\overline{\big(V\tilde{H}_1(s_1)\big)\otimes\big(V\tilde{H}_2(s_2,s_3)\big)}.\end{aligned} \tag{37}$$

As seen from the above equations, to compute the third-order transfer function, one needs to solve a linear system in terms of $\overline{G_1}$ and $\overline{C_1}$, and form the input to the linear system in terms of g that is a function of high-order system matrices $\overline{G_2},\overline{C_2},\overline{G_3},\overline{C_3}$ and low-order transfer functions $\overline{H_1},\overline{H_2}$. As $\overline{H_1},\overline{H_2}$ are approximated using (34), to further reduce (36) requires reduction of the dimension of the linear problem in (36) as well as the high-order system matrices $\overline{G_2},\overline{C_2},\overline{G_3},\overline{C_3}$. This goal is accomplished by a combination of projection-based reduction of an adjoint network and direct matrix pruning.

In analog signal processing and RF applications, a circuit block usually has only one or at most a few output nodes. For periodically time-varying systems, typically only a small number of sidebands (with respect to clock or LO) for the outputs are of interest. Thus, (36) can be viewed as a system with potentially many inputs but few outputs, and can be reduced as an adjoint network. Without loss of generality, let us assume only the ith sideband of the voltage response at node p is of interest (e.g., $i=0,\pm1$). Define $l=[0\ 0\ \cdots\ 1\ \cdots\ 0]^T$ as a $N\times 1$ vector that has a 1 at the pth location and zeros at all other locations, and

$$\begin{aligned}&L = \mathrm{diag}(l^T,l^T,\ldots,l^T)\in R^{M\times NM}\\ &d = \Big[1\ e^{-j2\pi i/M}\ \cdots\ e^{-j2\pi(M-1)i/M}\Big]^T\Big/M,\quad b_a = L^T d.\end{aligned} \tag{38}$$

The ith sideband of the third-order transfer function at node p, y_{p_i}, (corresponding to the ith harmonic of the third order transfer function for node p) can be obtained from the adjoint network

$$\begin{cases}\left[\overline{G_1}^T+\tilde{s}\overline{C_1}^T\right]z(s_1,s_2,s_3)=b_a\\ y_{p_i}=g^Tz\end{cases}. \tag{39}$$

We can apply Krylov subspace projection (such as [6]) to reduce the linear adjoint network of (39)

$$\hat{G}_a = V_a^T\overline{G_1}^T V_a,\qquad \hat{C}_a = V_a^T\overline{C_1}^T V_a,\qquad \hat{b}_a = V_a^T b_a \tag{40}$$

where V_a is a orthonormal basis of the Krylov subspace $\mathrm{colspan}\{r_a, A_a r_a, A_a^2 r_a\ldots\}$ with $A_a = -\overline{G_1}^{-T}\overline{C_1}^T, r_a = \overline{G_1}^{-T}b_a$. As the DFT vector d is absorbed into b_a, to perform a real projection, b_a can be split into real and imaginary parts before reduction [24]. Based on (39)–(40), we can approximate y_{p_i} as

$$\hat{y}_{p_i} = g^T\hat{z},\quad \hat{z} = V_a[\hat{G}_a+\tilde{s}\hat{C}_a]^{-1}\hat{b}_a \tag{41}$$

To speed up the computation of the third-order transfer function or response, high-order system matrices $\overline{G_2},\overline{C_2},\overline{G_3},\overline{C_3}$ need to be reduced. To avoid forming dense reduced matrices (particularly for the third-order ones) in a projection-based approach, here, we exploit the internal structure of the problem by applying a direct matrix pruning technique, where nonzero elements of $\overline{G_2},\overline{C_2},\overline{G_3},\overline{C_3}$ are pruned according to their contributions to the third order tranfer function at the output node of interest. Although a nonlinear circuit may contain many nonlinearities, a few of them tend to be dominant. Therefore, retaining

the original circuit structural information by avoiding using projection, and applying pruning to these high-order matrices in the original coordinates can be very effective for model generation. A similar idea has been used in symbolic modeling of nonlinear circuits, where dominant circuit nonlinearities are identified and kept for building system-level models [22], [23], [30], [31].

The matrix-pruning process proceeds as follows: A set of sampled frequency points Ω are first selected within the frequency band of interest. Then, for each of these frequency samples, the third order transfer function is computed, as well as the individual contributions of nonzeros in $\overline{G_2}, \overline{C_2}, \overline{G_3}, \overline{C_3}$. These contributions are sorted by magnitude, and nondominant ones are discarded provided that a user-specified error tolerance on H_3 is not exceeded. Notice that the pruning is performed directly on matrices. A matrix entry is discarded if and only if its removal does not violate the model accuracy at all the frequency points. The end products of the process are a set of pruned matrices $\overline{G_{2p}}, \overline{C_{2p}}, \overline{G_{3p}}, \overline{C_{3p}}$ that satisfy the error tolerance for all the sampled frequency points in Ω. Notice that these pruned high order system matrices retain the same dimensions as in the original system while their sparsity can be significantly improved as a result of pruning. As the computation of H_3 and individual contributions may take place on many sample points, matrix pruning can be a slow process. To speed up this process, we embed the projection-based model reduction step directly into the pruning procedure.

To compute H_3 at a frequency point, H_1 and H_2 need to be computed at related points. As in (37), to form vector g, we can use the reduced-order model in (33) and (34) to compute approximate first- and second-order transfer functions. Then, instead of solving a potentially large linear problem in (36), the reduced adjoint network of (41) can be used to find an approximate vector $\hat{z}$. Computation of each individual contribution term is straightforward, based on (37) and (41). For instance, the contribution of the nonzero at (m, n) location of $\overline{G_3}$ can be simply computed as

$$\delta_{g_3,m,n} = \overline{G_{3,m,n}} \cdot u_{1,n} \cdot \hat{z}_m \tag{42}$$

where $\overline{G_{3,m,n}}$ is the value of the nonzeo, $u_{1,n}$ is the nth element of u_1, and $\hat{z}_m$ is the mth element of $\hat{z}$. Since reduced order models are used, factorizing the original large system matrices at many sampled points are avoided. The cost for constructing projection-based reduced-order models of (33) and (41) is dominated by the cost of a few matrix factorizations, therefore it is bounded by $O(kM^3N^3)$, where k is the number of matrix factorizations, M is the number of sampled points used to discretize the periodically time-varying transfer functions, and N is the number of physical circuit unknowns. The cost of the pruning process is dominated by evaluation and sorting of the different contributions, assuming that the use of reduced order models makes other cost much less. The overall cost for model generation is, therefore, bounded by $O(sE\log(E)+kM^3N^3)$, where s is the number frequency samples evaluated in the pruning, and E is the number of nonzeros in the high order matrices being pruned.

Using the pruned matrices $\overline{G_{2p}}, \overline{C_{2p}}, \overline{G_{3p}}, \overline{C_{3p}}$, (37) can be further approximated as

$$\hat{g} = -[\overline{G_{3p}} + \tilde{s}\overline{C_{3p}}] \cdot \overline{\left(V\tilde{H}_1(s_1)\right) \otimes \left(V\tilde{H}_1(s_2)\right) \otimes \left(V\tilde{H}_1(s_3)\right)} - 2 \cdot [\overline{G_{2p}} + \tilde{s}\overline{C_{2p}}] \cdot \overline{\left(V\tilde{H}_1(s_1)\right) \otimes \left(V\tilde{H}_2(s_2, s_3)\right)}. \tag{43}$$

To derive a time-domain model for generating the desired third-order response, we substitute (43) into (41) and transpose both sides of the equation

$$\hat{y}_{p_i} = \hat{b}_a^T \left[\hat{G}_a^T + \tilde{s}\hat{C}_a^T\right]^{-1} V_a^T \hat{g}. \tag{44}$$

Defining

$$\begin{aligned} \overline{x_{111}} &= V\tilde{x}_1 \otimes V\tilde{x}_1 \otimes V\tilde{x}_1 \\ \overline{x_{12}} &= \frac{1}{2}(V\tilde{x}_1 \otimes V\tilde{x}_2 + V\tilde{x}_2 \otimes V\tilde{x}_1) \end{aligned} \tag{45}$$

it is not hard to show that the corresponding time-domain model is (see (46) at the bottom of the page) where $\tilde{x}_1, \tilde{x}_2$ are given in (35), $\tilde{y}_{p,3}(t)$ is the desired time-domain third-order response. Note that since only the ith harmonics of the third order transfer functions are considered at the output, $\hat{y}_{p,3}(t)$ in the above equation is complex. To recover the corresponding real signal, we can simply add the corresponding conjugate component. The first- and second-order responses at node p, $\hat{y}_{p,1}(t)$, and $\hat{y}_{p,2}(t)$, can be obtained from (35) by selecting the proper entries from $\tilde{y}$. Also note that when more than one output or set of side bands are of interest, multiple reduced adjoint networks can be incorporated into the model in a straightforward way.

C. Results

Switched-capacitor filters are often found in RF receivers as channel-select filters [25]. If the input signal is small, then these circuits can be characterized by periodically time-varying Volterra series. Due to the typical sharp transition between the passband and stopband, it can be very difficult to apply a full-projection-based model reduction.

To demonstrate the proposed hybrid approach, let us consider a Butterworth lowpass switched-capacitor biquad that is shown in Fig. 9. The two-phase clock is at 20 MHz, and the 3-dB frequency of the filter is about 700 KHz. Each circuit nonlinearity in the filter is modeled as a third-order polynomial

$$\begin{cases} \dfrac{d}{dt}\left(\hat{C}_a^T x_a\right) + \hat{G}_a^T x_a \\ = -V_a^T \left(\overline{G_{3p}} \cdot \overline{x_{111}} + \dfrac{d}{dt}(\overline{C_{3p}} \cdot \overline{x_{111}}) + 2\overline{G_{2p}} \cdot \overline{x_{12}} + 2\dfrac{d}{dt}(\overline{C_{2p}} \cdot \overline{x_{12}})\right), \\ \hat{y}_{p,3}(t) = e^{ji\omega_0 t}\hat{b}_a^T x_a \end{cases} \tag{46}$$

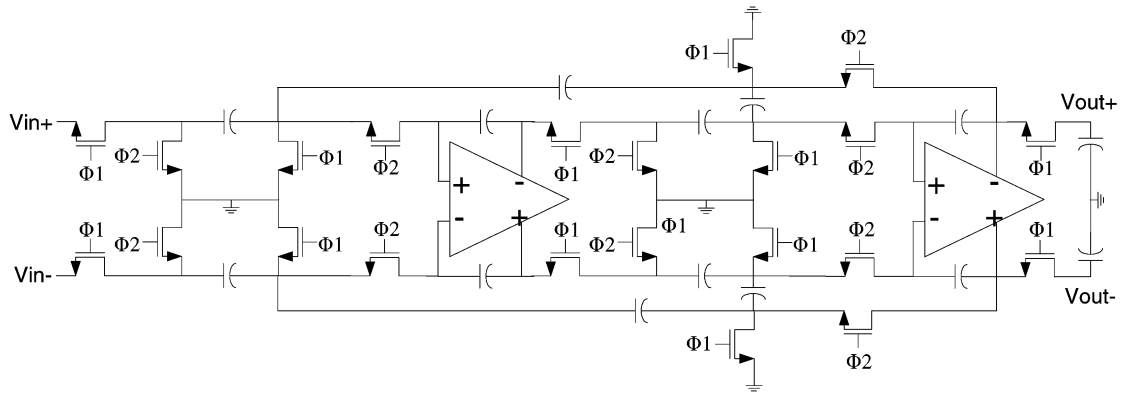

Fig. 9. Switched-capacitor biquad low-pass filter.

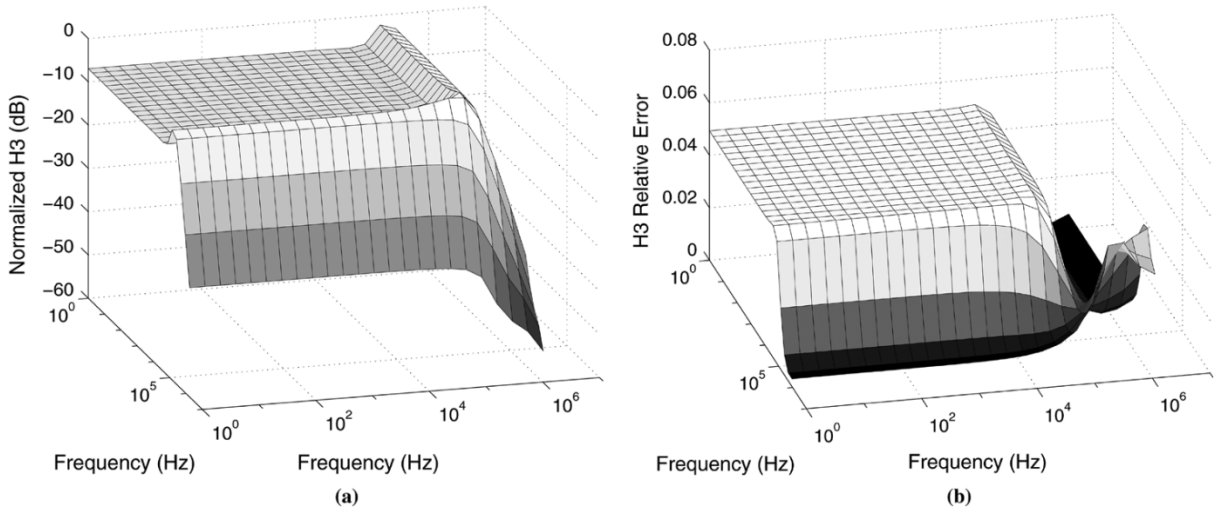

Fig. 10. (a) Original H_3 of the biquad. (b) Relative error of the reduced order model.

about the periodically varying operating point generated by the clock. The resulting full model has 8142 time-sampled circuit unknowns. To view the third-order nonlinear effects within and close to the signal band, we plot the dc component of the periodically time-varying third order nonlinear transfer function $H_3(t, j2\pi f_1, j2\pi f_2, j2\pi f_3)$, where 1 Hz $\leq f_1, f_2 \leq$ 10 MHz, $f_3 = -1$ Hz, in Fig. 10(a). It is clearly observable that the third order nonlinear characteristics vary dramatically between passband and stopband. To capture not only the nonlinear distortions due to the signals within the passband, but also the third order mixing of the large out of channel interferers into the passband, the nonlinear frequency-domain characteristics of the filter must be modeled accurately over a frequency range of seven decades. As such, a complete projection-based approach becomes inefficient, since a sufficient number of moments have to be matched for accuracy, while the resulting model size leads to expensive dense projected third order matrices.

To apply our hybrid approach, we first used the multipoint NORM algorithm to accurately capture the first and second transfer functions using a reduced-order model with 27 states (SVD was used to deflate the Krylov subspaces), where six moments of H_1 and 24 moments of H_2 were matched. The adjoint network describing the propagation of third-order nonlinear effects from various nonlinearities to the output was reduced to an eleventh-order model. Based on these reduced models, $\overline{G_2}, \overline{C_2}, \overline{G_3}, \overline{C_3}$ were significantly pruned in the original coordinates at 225 frequency points. Running on an IBM RS6000 workstation, it took 342 CPU s to complete the model generation. The overall runtime was dominated by the time spent in pruning. Therefore, the tradeoff between runtime and accuracy can be made by selecting an appropriate number of frequency points used for pruning. The original second- and third-order system matrices have 45 221 and 84 521 nonzeros, while the pruned matrices have only 196 and 430 nonzeros, respectively. The final hybrid model has a maximum relative modeling error less than 6% (or about 0.5 dB) for H_3, as shown in Fig. 10(b).

This hybrid model was also validated in a frequency-domain Volterra-like simulation using MATLAB, where six sinusoidals with various phases were selected from passband, transition band and stopband as input signals. The simulation result was compared against that of the full model, as shown in Fig. 11. As can be seen from the figure, the hybrid model captures the frequency-domain nonlinear characteristics of the filter over a wide range of input band very accurately. It took 1400 s to simulation the full mode, while the runtime of the reduced model was only 23 s. In this example, only a small number of input frequencies were considered in the frequency-domain

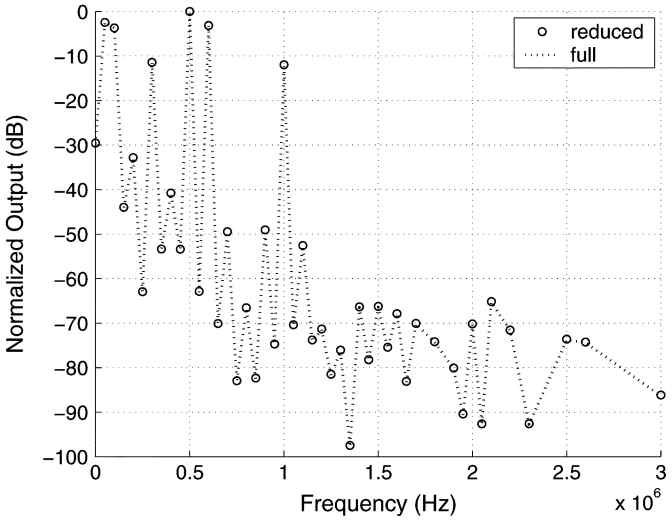

Fig. 11. Biquad output due to a six-tone sinusoidal input.

Volterra-like simulation. With respect to the model generation time, we expect the saving in simulation time would be more significant for time-domain simulations and larger frequency-domain simulations where many input frequencies are included.

VII. Conclusion

We have demonstrated that the rapid growth of reduced-order models for weakly nonlinear systems makes model order reduction much more difficult than for the case of LTI system-order reduction. This new challenge originates from the fact the complex nonlinear system effects must be encapsulated in the reduced-order model in addition to the first order system properties. The proposed nonlinear system order reduction algorithm (NORM) that is based on using a set of minimum Krylov subspaces for moment matching of nonlinear transfer functions, is shown to produce very compact macromodels. We have also demonstrated that for nonlinear reduction problems, multipoint expansion methods can further increase the model compactness at the expense of more matrix factorizations. Additionally, a hybrid approach was developed to overcome limitations of a full projection-based approach for cases where system nonlinear characteristics is coupled with sharp frequency selectivity. We have shown the efficacy and practical utility of presented nonlinear macromodeling techniques on various circuit examples.

Appendix

A. Proof of Theorem 1

Proof: Since the subspace $K_{k_1+1}(A, r_1)$ is contained in the space spanned by V, (30) is valid as proven in [6]. To prove (31), first notice that any $M_{2,l,m}(l \le k_2)$ can be expressed as a linear combination of Krylov subspace vectors in Table II. Therefore, it suffices to only show that all the Krylov vectors in Table II are preserved through the projection. For any Krylov subspace $K_i = K_{m_i}(A, v_i)$ in $K2(k_2)$, where v_i takes the either the form $G_1^{-1}G_2\overline{A^{m\otimes n}}r_2(m+n+m_i-1=k_2)$ or $G_1^{-1}C_2\overline{A^{m\otimes n}}r_2(m+n+m_i=k_2)$, using induction we show its Krylov vectors are preserved in the projection, i.e.,

$$A^l v_i = V\tilde{A}^l\tilde{v}_i, \quad 0 \le l \le m_i - 1. \tag{47}$$

Without loss of generality, consider the former case where $v_i = G_1^{-1}G_2\overline{A^{m\otimes n}}r_2$. For the reduced order model, we write

$$\begin{aligned}\tilde{v}_i &= \tilde{G}_1^{-1}\tilde{G}_2\overline{\tilde{A}^{m\otimes n}}\tilde{r}_2\\ \tilde{G}_1\tilde{v}_i &= \tilde{G}_2\overline{\tilde{A}^{m\otimes n}}\tilde{r}_2.\end{aligned} \tag{48}$$

Substituting both (29) and (30) into (48), we obtain

$$\begin{aligned}&V^TG_1V\tilde{v}_i\\ &\quad= \frac{1}{2}V^TG_2(V\otimes V)\big((\tilde{A}^m\tilde{r}_1)\otimes(\tilde{A}^n\tilde{r}_1)\\ &\qquad+(\tilde{A}^n\tilde{r}_1)\otimes(\tilde{A}^m\tilde{r}_1)\big)\\ &\quad= \frac{1}{2}V^TG_2\big((V\tilde{A}^m\tilde{r}_1)\otimes(V\tilde{A}^n\tilde{r}_1)\\ &\qquad+(V\tilde{A}^n\tilde{r}_1)\otimes(V\tilde{A}^m\tilde{r}_1)\big)\\ &\quad= \frac{1}{2}V^TG_2\big((A^mr_1)\otimes(A^nr_1)+(A^nr_1)\otimes(A^m\tilde{r}_1)\big).\end{aligned} \tag{49}$$

For the original system, similar to (48), we have

$$G_1v_i = \frac{1}{2}G_2\big((A^mr_1)\otimes(A^nr_1)+(A^nr_1)\otimes(A^mr_1)\big). \tag{50}$$

Since V is an orthnormal basis for the subspaces, v_i can be expressed as a unique linear combination of column vectors of V

$$v_i = V\hat{v}. \tag{51}$$

Substituting (51) into (50) and multiplying both sides of the equation by V^T, we get

$$\begin{aligned}V^TG_1V\hat{v} = \frac{1}{2}V^TG_2\big((A^mr_1)\otimes(A^nr_1)\\ +(A^nr_1)\otimes(A^mr_1)\big).\end{aligned} \tag{52}$$

Assume V^TG_1V is full-rank (the reduced system has defined dc solutions). Comparing (52) with (49), it is apparent that $\hat{v} = \tilde{v}_i$, or $v_i = V\tilde{v}_i$, i.e., (47) holds for $l = 0$. Now, suppose (47) holds for an arbitrary $l = p < m_i - 1$, we have

$$A^pv_i = V\tilde{A}^p\tilde{v}_i \tag{53}$$

$$A^{p+1}v_i = AV\tilde{A}^p\tilde{v}_i. \tag{54}$$

Again, we can express $A^{p+1}v_i$ as a unique linear combination of column vectors of V as $A^{p+1}v_i = V\hat{v}_{p+1}$, then after multiplying both sides by V^T, (54) becomes

$$V^TV\hat{v}_{p+1} = \hat{v}_{p+1} = V^TAV\tilde{A}^p\tilde{v}_i = \tilde{A}^{p+1}\tilde{v}_i \tag{55}$$

which is the same as $A^{p+1}v_i = V\tilde{A}^{p+1}\tilde{v}_i$. By induction, (47) is true for all $l, 0 \le l \le m_i - 1$, i.e., (31) is proven. Similarly, (32) can be shown. QED.

B. Reduction of Periodically Time-Varying Weakly Nonlinear Systems

In this Appendix, we show the extension to the reduction of periodically time-varying weakly nonlinear systems. To this end, we shall formulate the periodically time-varying nonlinear transfer functions in a proper matrix form such that essentially the same procedure used for time-invariant systems can be applied to reduce a periodically time-varying nonlinear system to a system of smaller size.

Consider applying a large excitation u_L (e.g., the LO in a mixer) to the system specified in (1), where u_L is a periodic signal with a period of T. The large excitation u_L introduces a periodically time-varying operating point to the small-signal input of the circuit (e.g., the small RF signal to a mixer). To perform a small-signal analysis while taking into account weak nonlinearities, expand the system differential equations in (1) along the T-periodic time-varying operating point due to u_L using a Taylor series

$$\begin{aligned}&\frac{d}{dt}\big(C_1(t)x + C_2(t)(x\otimes x) + C_3(t)(x\otimes x\otimes x) + \cdots\big)\\&\quad + G_1(t)x + G_2(t)(x\otimes x)\\&\quad + G_3(t)(x\otimes x\otimes x) + \cdots = bu_s(t)\end{aligned} \tag{56}$$

where u_s is the small-signal input to the system, $G_i(t)$ and $C_i(t)$ are the T-periodic time-varying conductance and capacitance matrices.

As an extension to the time-invariant case, T-periodic time-varying transfer functions $H_1(t,s), H_2(t,s_1,s_2)$, and $H_3(t,s_1,s_2,s_3)$ etc. can be used to describe the system in (56). The linearized system corresponding to (56) is a linear periodically time-varying (LPTV) system and is obtained by dropping higher order terms in (56)

$$\frac{d}{dt}\big(C_1(t)x(t)\big) + G_1(t)x = bu_s(t). \tag{57}$$

The LPTV transfer function $H_1(t,s)$ of (57) is determined by

$$G_1(t)H_1(t,s) + \frac{d}{dt}\big(C_1(t)H_1(t,s)\big) + sC_1(t)H_1(t,s) = b. \tag{58}$$

Use a backward-Euler discretization over M collocation time points $[t_1, t_2, \ldots t_M]$ within one period of the varying operating point, the LPTV transfer function $H_1(t,s)$ of (58) is given by [8], [17]

$$[\hat{J}_1 + s\hat{C}_1]H_1(s) = \hat{b} \tag{59}$$

where $\hat{H}_1(s) = [H_1^T(t_1,s), H_1^T(t_2,s), \ldots, H_1^T(t_M,s)]^T$ are M samples of $H_1(t,s)$

$$\hat{G}_1 = \begin{bmatrix} G_1(t_1) & & & \\ & G_1(t_2) & & \\ & & \ddots & \\ & & & G_1(t_M)\end{bmatrix}$$
$$\hat{C}_1 = \begin{bmatrix} C_1(t_1) & & & \\ & C_1(t_2) & & \\ & & \ddots & \\ & & & C_1(t_M)\end{bmatrix} \tag{60}$$

$$\Delta = \begin{bmatrix} \frac{1}{h_1}I & & & -\frac{1}{h_1}I \\ -\frac{1}{h_2}I & \frac{1}{h_2}I & & \\ & \ddots & \ddots & \\ & & -\frac{1}{h_M}I & \frac{1}{h_M}I\end{bmatrix}$$
$$h_i = \begin{cases} t_1 + T - t_M, & i = 1 \\ t_i - t_{i-1} & 2 \le i \le M\end{cases} \tag{61}$$

and

$$\hat{J}_1 = \hat{G}_1 + \Delta\hat{C}_1, \quad \hat{b} = [b^T, b^T, \ldots, b^T]^T. \tag{62}$$

Additionally, the output matrix associated with this time-domain discretization is $\hat{D} = \mathrm{diag}(D, D, \ldots, D)$.

To derive the second- and third-order matrix-form periodically time-varying nonlinear transfer functions, in contrast to (17) and (18) of the time-invariant case, we have

$$\begin{aligned}&[G_1(t) + \tilde{s}C_1(t)]H_2(t,s_1,s_2) + \frac{d}{dt}[C_1(t)H_2(t,s_1,s_2)]\\&\quad = -[G_2(t) + \tilde{s}C_2(t)]\overline{H_1(t,s_1)\otimes H_1(t,s_2)}\\&\qquad + \frac{d}{dt}[C_2(t)\overline{H_1(t,s_1)\otimes H_1(t,s_2)}]\end{aligned} \tag{63}$$

and

$$\begin{aligned}&[G_1(t) + \tilde{s}C_1(t)]H_3(t,s_1,s_2,s_3) + \frac{d}{dt}[C_1(t)H_3(t,s_1,s_2,s_3)]\\&\quad = -2[G_2(t) + \tilde{s}C_2(t)]\overline{H_1(t,s_1)\otimes H_2(t,s_2,s_3)}\\&\qquad - [G_3(t) + \tilde{s}C_3(t)]\overline{H_1(t,s_1)\otimes H_1(t,s_2)\otimes H_1(t,s_3)}\\&\qquad - \frac{d}{dt}[2C_2(t)\overline{H_1(t,s_1)\otimes H_2(t,s_2,s_3)}]\\&\qquad + C_3(t)\overline{H_1(t,s_1)\otimes H_1(t,s_2)\otimes H_1(t,s_3)}]\end{aligned} \tag{64}$$

where $\bar{s} = s_1 + s_2$, $\tilde{s} = s_1 + s_2 + s_3$, $\overline{H_1(t,s_1)\otimes H_2(t,s_2,s_3)}$, and $\overline{H_1(t,s_1)\otimes H_1(t,s_2)\otimes H_1(t,s_3)}$ are defined as the arithmetic average of the terms due to the permutations of the frequency variables. Now, for the second-order periodically time-varying transfer functions of (63), a backward-Euler discretization yields

$$[\hat{J}_1 + \bar{s}\hat{C}_1]\hat{H}_2(s_1,s_2) = -[\hat{J}_2 + \bar{s}\hat{C}_2]\tilde{H}_1 \tag{65}$$

where $\hat{H}_2(s_1,s_2) = [H_2^T(t_1,s_1,s_2), H_2^T(t_2,s_1,s_2), \ldots, H_2^T(t_M,s_1,s_2)]^T$ are M samples of $H_2(t,s_1,s_2)$ within one period

$$\hat{G}_2 = \begin{bmatrix} G_2(t_1) & & & \\ & G_2(t_2) & & \\ & & \ddots & \\ & & & G_2(t_M)\end{bmatrix}$$
$$\hat{C}_2 = \begin{bmatrix} C_2(t_1) & & & \\ & C_2(t_2) & & \\ & & \ddots & \\ & & & C_2(t_M)\end{bmatrix}$$
$$\hat{J}_2 = \hat{G}_2 + \Delta\hat{C}_2 \tag{66}$$
$$\tilde{H}_1 = \left[\tilde{h}_1^T, \tilde{h}_2^T, \ldots, \tilde{h}_M^T\right] \tag{67}$$
$$\tilde{h}_i = \overline{H_1(t_i,s_1)\otimes H_1(t_i,s_2)}. \tag{68}$$

Note that $\hat{H}_2(s_1,s_2) \in \Re^{NM\times 1}$, but the dimension of matrices $\hat{G}_2$ and $\hat{C}_2$ is $NM \times N^2M$ instead of $NM \times N^2M^2$, where

N is the number of circuit unknowns. Thus, (66) is a compact representation of the second order transfer function.

Similarly for the third order nonlinear transfer functions, define

$$\tilde{H}_{12} = \left[\tilde{h}_{12,1}^T, \tilde{h}_{12,2}^T, \ldots, \tilde{h}_{12,M}^T\right] \quad \text{with}$$
$$\tilde{h}_{12,i} = \overline{H_1(t_i, s_1) \otimes H_2(t_i, s_2, s_3)} \tag{69}$$
$$\tilde{H}_{111} = \left[\tilde{h}_{111,1}^T, \tilde{h}_{111,2}^T, \ldots, \tilde{h}_{111,M}^T\right] \quad \text{with}$$
$$\tilde{h}_{111,i}^T = \overline{H_1(t_i, s_1) \otimes H_1(t_i, s_2) \otimes H_1(t_i, s_3)} \tag{70}$$
$$\hat{G}_3 = \begin{bmatrix} G_3(t_1) & & & \\ & G_3(t_2) & & \\ & & \ddots & \\ & & & G_3(t_M) \end{bmatrix}$$
$$\hat{C}_3 = \begin{bmatrix} C_3(t_1) & & & \\ & C_3(t_2) & & \\ & & \ddots & \\ & & & C_3(t_M) \end{bmatrix}$$
$$\hat{J}_3 = \hat{G}_3 + \Delta\hat{C}_3. \tag{71}$$

Discretizing (64) using backward-Euler leads to

$$[\hat{J}_1 + \tilde{s}\hat{C}_1]\hat{H}_3(s_1, s_2, s_3) = -2[\hat{J}_2 + \tilde{s}\hat{C}_2]\tilde{H}_{12} - [\hat{J}_3 + \tilde{s}\hat{C}_3]\tilde{H}_{111}. \tag{72}$$

Notice that (66) and (72) are in the same structure as (17) and (18), respectively, therefore, the previously presented model order-reduction approach can be directly applied. Now, assume that the system matrices $\hat{G}_1, \hat{C}_1, \hat{b}, \hat{D}, \hat{G}_2, \hat{C}_2, \hat{G}_3, \hat{C}_3$ of the original periodically time-varying systems specified are reduced to $\tilde{G}_1, \tilde{C}_1, \tilde{b}, \tilde{D}, \tilde{G}_2, \tilde{C}_2, \tilde{G}_3, \tilde{C}_3$, a set of matrices of smaller dimensions, using NORM. It can be shown that a time-domain realization of the above-reduced model matches the moments of original periodically time-varying transfer functions in the sense of Definition 1 is

$$\frac{d}{dt}\left(\tilde{C}_1 x + \tilde{C}_2(\tilde{x} \otimes \tilde{x}) + \tilde{C}_3(\tilde{x} \otimes \tilde{x} \otimes \tilde{x})\right) + \tilde{G}_1\tilde{x} + \tilde{G}_2(\tilde{x} \otimes \tilde{x}) + \tilde{G}_3(\tilde{x} \otimes \tilde{x} \otimes \tilde{x}) = \tilde{b}u(t) \tag{73}$$
$$\tilde{y}(t) = \tilde{l}(t)\tilde{x}(t) \tag{74}$$

where $\tilde{l}(t) = [\ldots, e^{-j2\pi f_0 t}, e^0, e^{j2\pi f_0 t}, \ldots] \cdot \Gamma \cdot \tilde{D}^T$ in which Γ is the DFT matrix converting a vector of M time samples to the corresponding Fourier coefficients, $f_0 = (1/T)$ is the frequency of the periodically time-varying operating point.

REFERENCES

[1] L. Pillage and R. Rohrer, "Asymptotic waveform evaluation for timing analysis," *IEEE Trans. Computer-Aided Design Integr. Circuits Syst.*, vol. 9, no. 4, pp. 352–366, Apr. 1990.

[2] E. Chiprout and M. Nakhla, "Analysis of interconnect network using complex frequency hopping (CFH)," *IEEE Trans. Computer-Aided Design Integr. Circuits Syst.*, vol. 14, no. 2, pp. 186–200, Feb. 1995.

[3] P. Feldmann and R. Freund, "Efficient linear circuit analysis by Padé approximation via the Lanczos process," *IEEE Trans. Computer-Aided Design Integr. Circuits Syst.*, vol. 14, no. 5, pp. 639–649, May 1995.

[4] L. Silveira, M. Kamon, and J. White, "Efficient reduced-order modeling of frequency-dependent coupling inductances associated with 3-D interconnect structures," *IEEE Trans. Compon. Packag. Manuf. Technol. A*, pt. B, vol. 19, no. 2, pp. 283–288, May 1996.

[5] K. J. Kerns and A. T. Yang, "Stable and efficient reduction of large, multiport RC networks by poles analysis via congruence transformations," *IEEE Trans. Computer-Aided Design Integr. Circuits Syst.*, vol. 16, no. 7, pp. 734–744, Jul. 1997.

[6] A. Odabasioglu, M. Celik, and L. Pileggi, "PRIMA: Passive reduced-order interconnect macromodeling algorithm," *IEEE Trans. Computer-Aided Design Integr. Circuits Syst.*, vol. 17, no. 8, pp. 645–653, Aug. 1998.

[7] J. Phillips, L. Daniel, and M. Silveira, "Guaranteed passive balancing transformations for model order reduction," in *Proc. IEEE/ACM Design Automation Conf.*, Jun. 2002, pp. 52–57.

[8] J. Roychowdhury, "Reduced-order modeling of time-varying systems," *IEEE Trans. Circuits Syst. II: Analog Digital Signal Process.*, vol. 46, no. 10, pp. 1273–1288, Oct. 1999.

[9] J. Phillips, "Projection frameworks for model reduction of weakly nonlinear systems," in *Proc. IEEE/ACM Design Automaton Conf.*, Jun. 2000, pp. 184–189.

[10] ——, "Automated extraction of nonlinear circuit macromodels," in *Proc. Custom Integr. Circuits Conf.*, May 2000, pp. 451–454.

[11] M. Rewienski and J. White, "A trajectory piecewise-linear approach to model order reduction and fast simulation of nonlinear circuits and micromachined devices," in *Proc. IEEE/ACM Int. Conf. Computer-Aided Design*, Nov. 2001, pp. 252–257.

[12] J. Bussgang, L. Ehrman, and J. Graham, "Analysis of nonlinear systems with multiple inputs," *Proc. IEEE*, vol. 62, no. 8, pp. 1088–1119, Aug. 1974.

[13] D. Wiener and J. Spina, *Sinusoidal Analysis and Modeling of Weakly Nonlinear Circuits*. New York: Reinhold, 1980.

[14] S. A. Maas, *Nonlinear Microwave Circuits*. Norwood, MA: Artech House, 1988.

[15] R. Telichevesky, K. Kundert, and J. White, "Efficient AC and noise analysis of two-tone RF circuits," in *Proc. IEEE/ACM Design Automation Conf.*, Jun. 1996, pp. 292–297.

[16] M. Terrovitis and R. Meyer, "Intermodulation distortion in current-commutating CMOS mixers," *IEEE J. Solid-State Circuits*, vol. 35, no. 10, pp. 1461–1473, Oct. 2000.

[17] J. Phillips, "Model reduction of time-varying linear systems using approximate multipoint Krylov-subspace projectors," in *Proc. IEEE/ACM Int. Conf. Computer-Aided Design*, Nov. 1998, pp. 96–102.

[18] P. Li and L. Pileggi, "NORM: Compact model order reduction of weakly nonlinear systems," in *Proc. ACM/IEEE Design Automation Conf.*, Jun. 2003, pp. 472–477.

[19] P. Li, X. Li, Y. Xu, and L. Pileggi, "A hybrid approach to nonlinear macromodel generation for time-varying analog circuits," in *Proc. ACM/IEEE Int. Conf. Computer-Aided Design*, Nov. 2003, pp. 454–461.

[20] F. Liu and E. Acar, private communication, 2002.

[21] Y. Chen and J. White, "A quadratic method for nonlinear model order reduction," presented at the Int. Conf. Modeling Simul. Microsyst., Mar. 2000.

[22] P. Wambacq and W. Sansen, *Distortion Analysis of Analog Integrated Circuits*. Norwell, MA: Kluwer, 1998.

[23] P. Wambacq, P. Dobrovolny, S. Donnay, M. Engels, and I. Bolsens, "Compact modeling of nonlinear distortion in analog communication circuits," in *Proc. ACM/IEEE Design, Automation Test Eur. Conf.*, Mar. 2000, pp. 350–354.

[24] A. Ruhe, "The rational Krylov algorithm for nonsymmetric eigenvalue problems III: Complex shifts for real matrices," *BIT*, vol. 34, pp. 165–176, 1994.

[25] P. Chang, A. Rofougaran, and A. Abidi, "A CMOS channel-select filter for a direct-conversion wireless receiver," *IEEE J. Solid-State Circuits*, vol. 32, no. 5, pp. 722–729, May 1997.

[26] J. Phillips, "Projection-based approaches for model reduction of weakly, time-varying systems," *IEEE Trans. Computer-Aided Design Integr. Circuits Syst.*, vol. 22, no. 2, pp. 171–187, Feb. 2003.

[27] N. Dong and J. Roychowdhury, "Piecewise polynomial nonlinear model reduction," in *Proc. ACM/IEEE Design Automation Conf.*, Jun. 2003, pp. 484–489.

[28] D. Root, J. Wood, and N. Tufillaro, "New techniques for nonlinear behavioral modeling of microwave/RF ICS from simulation and nonlinear microwave measurements," in *Proc. ACM/IEEE Design Automation Conf.*, Jun. 2003, pp. 85–90.

[29] Matlab Simulink Reference [Online]. Available: http://www.mathworks.com/
[30] S. Seda, M. Degrauwe, and W. Fichtner, "A symbolic analysis tool for analog circuit design automation," in *Proc. ACM/IEEE Int. Conf. Computer-Aided Design*, Nov. 1988, pp. 488–491.
[31] G. Gielen, H. Walscharts, and W. Sansen, "ISAAC: A symbolic simulator for analog integrated circuits," *IEEE J. Solid-State Circuits*, vol. 24, no. 6, pp. 1587–1597, Dec. 1989.

Peng Li (S'02–M'04) received the B.Eng. degree in information engineering and the M.Eng. degree in systems engineering from Xi'an Jiaotong University, Xi'an, China, in 1994 and 1997, respectively, and the Ph.D. degree in electrical and computer engineering from Carnegie Mellon University, Pittsburgh, PA, in 2003.

From December 2003 to July 2004, he was a Post-Doctoral Research Associate in the Department of Electrical and Computer Engineering, Carnegie Mellon University. Since August 2004, he has been an Assistant Professor in the Department of Electrical Engineering, Texas A&M University, College Station. His research interests are in the various aspects of very large scale integrated computer-aided design with an emphasis on simulation and modeling of integrated circuits.

Dr. Li received the Inventor Recognition Awards from the Semiconductor Research Corporation in 2001 and 2004 and a Best Paper Award from the Design Automation Conference in 2003.

Lawrence T. Pileggi (S'85–M'89–SM'94–F'01) received the Ph.D. degree in electrical and computer engineering from Carnegie Mellon University, Pittsburgh, PA, in 1989.

He is the Tanoto Professor of electrical and computer engineering and the Director of the Center for Silicon System Implementation at Carnegie Mellon University, where he has been since 1996. From 1984 to 1986, he was with Westinghouse Research and Development, where, in 1986, he was recognized with the corporation's highest engineering achievement award. From 1989 to 1995, he was a Faculty Member at the University of Texas, Austin. He has consulted for several electronic design automation and semiconductor companies. He is a coauthor of "Electronic Circuit and System Simulation Methods," (New York: McGraw-Hill, 1995) and "IC Interconnect Analysis," (Norwell, MA: Kluwer, 2002). He has published over 175 refereed conference and journal papers and holds 13 U.S. patents. His research interests include various aspects of digital and analog design and electronic design automation (EDA).

Prof. Pileggi served as the Technical Program Chairman of the 2001 International Conference on Computer-Aided Design (ICCAD) and as the Conference Chairman of the 2002 ICCAD. He received the Best Computer-Aided Design Transactions Paper Awards in 1991 and 1999. In 2003, he received a Best Paper Award from DAC, and in 2004 he received a Best Paper Award from ICCAD. He received a Presidential Young Investigator Award from the National Science Foundation in 1991. In 1991 and 1999, he received the Semiconductor Research Corporation (SRC) Technical Excellence Award. In 1993, he received an Invention Award from the SRC. In 1994, he received The University of Texas Parent's Association Centennial Teaching Fellowship for excellence in undergraduate instruction. In 1995, he received a Faculty Partnership Award from IBM.